The level of Nck rather than N-WASP determines the rate of actin-based motility of Vaccinia

Angika Basant[1, *] and Michael Way[1, 2, *]

[1] Cellular signalling and cytoskeletal function laboratory, The Francis Crick Institute, 1 Midland
6 Road, London, NW1 1AT, UK

[2] Department of Infectious Disease, Imperial College, London, UK

*Co-corresponding.

Email: angika.basant@crick.ac.uk and michael.way@crick.ac.uk

12

Running title: Quantitative imaging of vaccinia virus stimulating actin polymerization

ABSTRACT

Vaccinia virus exiting from host cells activates Src/Abl kinases to phosphorylate A36, an
18 integral membrane viral protein. Phosphorylated A36 binds the adaptors Nck and Grb2 which recruit N-WASP to activate Arp2/3-driven actin polymerisation to promote viral spread. A36 also recruits intersectin, which enhances actin polymerization via AP-2/clathrin and Cdc42. To obtain a better quantitative understanding of this signalling network we still need to know the absolute numbers of the key molecules. To achieve this goal, we have now used fluorescent molecule counting approaches in live cells. There are 1156±120 A36 molecules
24 on virus particles inducing actin polymerization in HeLa cells. This number, however, is over 2000 in mouse embryonic fibroblasts (MEFs), suggesting that A36 levels on the virion are not fixed. In MEFs, viruses recruit 1032±200 Nck and 434±10 N-WASP molecules, suggesting a ratio of 4:2:1 for the A36:Nck:N-WASP signalling network. Loss of A36 binding to either Grb2 or intersectin results in a 1.3- and 2.5-fold reduction in Nck respectively. Despite recruiting comparable numbers of the Arp2/3 activator, N-WASP (245±26 and 276±66), these mutant
30 viruses move at different speeds that inversely correlate with the number of Nck molecules. Our analysis has uncovered two unexpected new aspects of Vaccinia egress, A36 levels can vary in the viral membrane and the velocity of virus movement depends on Nck.

INTRODUCTION

Vaccinia virus is the most studied member of the poxvirus family and best known for being
36 used as the vaccine to protect against smallpox. It is a large double stranded DNA virus, which undergoes a complex replication cycle in perinuclear cytoplasmic viral factories in infected cells (Leite & Way 2015). Replication results in the formation of infectious intracellular mature virions (IMV) which undergo kinesin-1 driven microtubule transport to disperse throughout the cell before being released when the infected host lyses (Sanderson et al. 2000; Ward 2005; Xu et al. 2022). Prior to cell lysis, some IMV are also capable of becoming enveloped
42 by a Golgi cisterna to form intracellular enveloped virions (IEV) (Leite & Way 2015; Schmelz et al. 1994; Tooze et al. 1993). This envelopment process, which is still not fully understood, is dependent on several viral proteins including the integral membrane protein B5 and the lipid-anchored F13 (Blasco & Moss 1991; Engelstad & Smith 1993; Smith et al. 2002; Wolffe et al. 1993). Once formed, IEV undergo microtubule-based transport from their perinuclear site of assembly to the plasma membrane (Geada et al. 2001; Hollinshead et al. 2001; Rietdorf
48 et al. 2001; Ward & Moss 2001a), where they fuse their outermost membrane to release extracellular enveloped virions (EEV) (Leite & Way 2015; Smith et al. 2002). EEV are thought to promote the long-range spread of infection, but some virions can remain attached to the outer surface of host cell after fusion. Known as cell-associated extracellular virions (CEV), these viruses can induce Arp2/3 complex dependent actin polymerisation beneath the virion (Fig 1), (Cudmore et al. 1995, 1996; Frischknecht et al. 1999; Hollinshead et al. 2001). The
54 power of actin polymerization subsequently drives the CEV away from the host cell to enhance its spread into non-infected neighbouring cells (Cudmore et al. 1995, 1996; Doceul et al. 2010; Ward & Moss 2001b).

The ability of IEV to move on microtubules as well as the stimulation of actin polymerization by CEV is dependent on A36, an integral viral membrane protein present in the Golgi that
60 envelopes IMV during IEV formation (Frischknecht et al. 1999; Rietdorf et al. 2001; Röttger et al. 1999; Sanderson et al. 1998; Ward & Moss 2001a; Wolffe et al. 1998). In contrast to B5 and other integral viral membrane proteins in the Golgi that wrap IMV, A36 does not end up in EEV and is only retained in the plasma membrane beneath CEV (Fig. 1), (Smith et al. 2002; van Eijl et al. 2000). A36 facilitates microtubule transport of IEV by recruiting kinesin-1 to the virus (Rietdorf et al. 2001). It achieves this by interacting directly with the tetratricopeptide

66 repeats (TPR) of the kinesin light chain via a bipartite tryptophan acidic motif that is also found in cellular kinesin-1 binding proteins (Dodding et al. 2011; Pernigo et al. 2013; Ward & Moss 2004). After IEV fuse with the plasma membrane, CEV attached to the outside of the cell locally activate Src and Abl family kinases to induce phosphorylation of tyrosine 112 and 132 in the cytosolic tail of A36 (Fig. 1), (Frischknecht et al. 1999; Newsome et al. 2004, 2006; Reeves et al. 2005). Phosphorylation of tyrosine 112 and 132, results in the recruitment of
72 the adaptors Nck and Grb2 via their SH2 domains respectively (Frischknecht et al. 1999; Scaplehorn et al. 2002). Nck subsequently recruits N-WASP via WIP to stimulate the actin nucleating activity of the Arp2/3 complex beneath CEV (Donnelly et al. 2013; Moreau et al. 2000; Zettl & Way 2002). The resulting actin polymerisation drives CEV motility, enhancing cell-to-cell spread of infection (Ward & Moss 2001a). Not surprisingly, the amount of phosphorylation competent A36 influences the length of actin tails as well as the speed of
78 virus movement (Humphries et al. 2012). Grb2, in contrast to Nck, is not essential for this process, but its recruitment stabilises the signalling complex, making actin assembly more robust (Scaplehorn et al. 2002; Weisswange et al. 2009). In addition, three NPF motifs near the C-terminus of A36 interact with the RhoGEF intersectin to recruit Cdc42 and clathrin, further enhancing actin polymerisation beneath CEV (Fig 1) (Humphries et al. 2012, 2014; Snetkov et al. 2016).

84

We know the identity of the viral and key host components as well as their interactions and roles in CEV-stimulated actin assembly. The turnover rates of Nck, Grb2, WIP and N-WASP beneath CEV have also been determined (Weisswange et al. 2009). However, to obtain a full quantitative understanding of virus induced actin polymerization we need to know the number of molecules participating in this signalling network. Taking advantage of fluorescent
90 nanocages with defined numbers of GFP molecules (Akamatsu et al. 2020), we recently determined that IEV recruit 320 kinesin-1 motor complexes (Xu et al. 2022). Using a similar approach, we have now determined the number of A36 molecules beneath CEV together with B5 and F13 which are essential for IEV assembly, as well as Nck and N-WASP that are required for CEV induced actin polymerization.

96

RESULTS

Quantification of the number of A36 molecules associated with CEV

To measure the number of A36 molecules on virus-induced actin tails using quantitative fluorescent imaging, we first generated a recombinant virus expressing an A36-TagGFP2
102 fusion from its genomic locus together with RFP-A3 to mark viral cores (Fig S1A). The A36-TagGFP2 recombinant virus formed plaques that were slightly smaller in diameter than the Western Reserve (WR) the parental strain (1.63±0.12 mm vs 1.95±0.07 mm) (Fig S1B). Importantly, A36-TagGFP2 was incorporated in late-stage virus particles which localized to the tip of actin tails (Fig 2A). The intensity of A36-TagGFP2 was substantially higher than membrane-tethered nanocages we have previously used to generate a fluorescence
108 calibration curve in live cells (Fig 2B, (Xu et al. 2022)). The upper limit of our calibration curve is 180 molecules (Fig S2A, (Xu et al. 2022)). To examine whether the curve we generated would be valid for higher fluorescence intensities, we acquired images of 60mer and 120mer nanocages at 4x and 3x exposure times respectively. The average measurements obtained from these experiments, were consistent with the expected values for a 240mer and 360mer nanocage (Fig 2C). To quantitively determine the number of A36 molecules on virus inducing
114 actin tails, we imaged and analysed confocal Z-stacks of HeLa cells infected with the A36-TagGFP2 virus from 8 hours post-infection, using LifeAct-iRFP and RFP-A3 as actin and viral markers respectively (Fig 2D). Co-localisation of A36-TagGFP2 and RFP-A3 signals occurs in IEV and CEV but the inclusion of an actin marker ensures that only CEV are analysed. This analysis revealed that CEV on the tips of actin tails have 1156 ± 120 A36 molecules. As this value is much higher than our experimentally established calibration curve, we also measured
120 A36-TagGFP2 intensities on actin tails at 0.5x and 0.25x exposure times (Fig 2D). The average intensity values obtained from these shorter exposure times lie along the extrapolated calibration curve, suggesting that our determination of A36 numbers is reliable.

Viral proteins F13 and B5 are present in high numbers on CEV

In addition to A36, the outer membrane of Vaccinia has additional viral proteins, A33, A34,
126 A56, E2, F12, B5 and F13, the latter two of which are required for formation of intracellular enveloped virions (IEV) the precursor to CEV (Dodding et al. 2009; Domi et al. 2008; Smith et al. 2002). B5, like A36 is an integral membrane protein, while F13 associates with the viral membrane via lipidation. Given the essential role of B5 and F13 in the assembly of IEV, the

precursor to CEV, we wondered how the abundance of B5 and F13 compares to A36. We therefore generated recombinant viruses expressing B5-TagGFP2 or TagGFP2-F13 at their
132 endogenous loci in a parental virus expressing RFP-A3 to determine the numbers of B5 and F13 molecules associated with CEV nucleating actin tails (Fig S1A). The B5-TagGFP2 and TagGFP2-F13 recombinant viruses also formed plaques that were slightly smaller than the parental Western Reserve (WR) strain (Fig S1B). B5-TagGFP2 and TagGFP2-F13 positive virus particles were observed at the tips of actin tails in infected cells, with TagGFP2-F13 appearing substantially brighter than B5-TagGFP2 (Fig 3A). To quantify their absolute numbers, we
138 imaged and analysed Z sections of infected cells as described for A36-TagGFP2. Based on comparisons of the fluorescence intensities obtained with our calibration curve, we calculated that CEV particles in HeLa cells inducing actin tails have 3107±602 and 8729±688 B5 and F13 molecules respectively (Fig 3B,C). These values are considerably higher than that of A36, however, B5 and F13 unlike A36 are present in the plasma membrane beneath CEV as well as the virion membrane (Fig 1).

144

What is the ratio of A36:Nck:N-WASP on virions nucleating actin?

Once phosphorylated, A36 recruits a signalling network involving the adaptor Nck and N-WASP to activate the Arp2/3 complex to induce an actin tail. Nck and N-WASP are essential for this process, but how many molecules of each do CEV recruit? To address this question, we generated cell lines stably expressing TagGFP2-Nck1 in mouse embryonic fibroblasts
150 (MEFs) lacking Nck1 and Nck2, as well as TagGFP2-N-WASP in N-WASP null MEFs (Fig S3). Using these cells ensures that all the Nck or N-WASP molecules are fluorescently labelled. However, these are a different host cell type from HeLa, which were used to determine the number of A36 molecules associated with CEV.

Virion composition and structure is not expected to vary depending on the host cell type, but
156 this has never formally been investigated. To determine whether A36 numbers are comparable between MEF and HeLa cells, we quantified A36-TagGFP2 molecules on virions inducing actin tails in Nck+/+ and N-WASP+/+ parental MEFs. Surprisingly, we find that the number of A36 molecules in both MEF cell lines is considerably higher than in HeLa cells (Fig 4A). We confirmed that nanocage intensities were comparable between these cell types (Fig S2B), suggesting that A36 incorporation into CEV is indeed higher in MEFs. We wondered

162 whether this difference relates to the cell type and/or host species. To test whether this is the case, we determined A36 numbers on virus inducing actin polymerization in human lung epithelial A549 cells. We found that CEV forming actin tails in A549 cells have comparable numbers of A36 molecules as we measured in HeLa (A549 1165±126 vs HeLa 1156 ± 120). We next sought to determine if these host-dependent differences are also true for B5. Measuring the intensity of B5-TagGFP2 on CEV in HeLa, A549 and the two MEF cell lines reveals that, in
168 contrast to A36, the numbers of B5 molecules are comparable between the four different cell lines (Fig 4B).

As the Vaccinia life-cycle appears to proceed faster in HeLa cells than MEFs, our lab typically analyses actin tails at 8 and 16 hours post-infection in these cell types respectively (Weisswange et al. 2009). To investigate whether A36 levels on CEV depends on time post-
174 infection, we compared A36-TagGFP2 intensities in HeLa and MEF cells at 8 and 16 hours post infection. We find that A36 numbers on CEV particles do not vary with time in HeLa cells. In contrast, in MEFs, the level of A36 associated with CEV increase as the infection progresses, but even at 8 hours post infection, more A36 molecules are present than in HeLa (Fig 4D). The reason for this difference is not immediately clear although it is striking that the bulk levels of A36, but not B5 are considerably higher in N-WASP+/+ parental MEFs than HeLa cells (Fig. 4E).
180

Having determined the number of A36 molecules on CEV in MEF cells, we measured the number of Nck and N-WASP molecules associated with the virus. TagGFP2 tagged Nck and N-WASP were both recruited to CEV inducing actin tails (Fig 5A). Quantification of the fluorescence intensity of the TagGFP2 signals in Z stacks indicates that each CEV recruits on average 1032 ± 200 and 434 ± 10 Nck and N-WASP molecules respectively (Fig 5C, D). Taken
186 together with our data on A36 numbers on actin tail forming particles in MEFs in Fig 4C, this suggests that A36, Nck and N-WASP are present in 4:2:1 ratio.

The level of Nck and not N-WASP determines the velocity of CEV

While Nck and N-WASP are essential for CEV induced actin polymerisation, the virus also recruits Grb2 and intersectin which act as secondary factors to enhance actin tail formation
192 (Fig 1). Our previous FRAP analysis demonstrates that Grb2 helps stabilize Nck and N-WASP beneath CEV during virus induced actin polymerization (Weisswange et al. 2009). To

determine whether these factors also impact on the number of Nck and N-WASP molecules, we infected cells with either the A36-Y132F or A36△NPF mutant viruses. Our measurements show that mutation of Tyr132 to phenylalanine (loss of Grb2) reduced the level of Nck and N-WASP by ~24% and 44% respectively N-WASP (Fig 6A,B). However, in the absence of the A36
198 NPF motifs, both Nck and N-WASP numbers were significantly reduced (~61 and 36%) (Fig 6A, B). Interestingly, for both the A36-Y132F and A36△NPF mutant viruses, the number of N-WASP molecules were reduced to similar levels (245 ± 26 and 276 ± 66 respectively).

Nck and N-WASP association with CEV generates Arp2/3-mediated actin polymerisation that drives the motility of the virus. As N-WASP directly activates the Arp2/3 complex, we would
204 predict that N-WASP numbers alone ultimately determine the speed of the virion. To examine if this is indeed the case, we measured the speed of wild-type, A36-Y132F and A36 △NPF viruses in HeLa cells stably expressing LifeAct-iRFP. Surprisingly, despite having similar levels of N-WASP, the A36-Y132F and A36△NPF viruses move at different speeds (Fig 6C). The A36-Y132F virus is slightly faster than the wildtype WR strain (0.2 ± 0.01 compared to 0.17 ± 0.01 μm/sec), but the speed of A36△NPF virus is significantly increased (0.24 ± 0.02
210 μm/sec). It is striking that these changes in virus speed are inversely proportional to the number of Nck molecules recruited by the virus.

DISCUSSION

Over the years, Vaccinia has provided a powerful model to understand the function and regulation of Nck:N-WASP signalling and its role in stimulating Arp2/3 driven actin
216 polymerization. Our current analysis provides new quantitative information concerning the signalling network driving this process. We found that Nck is twice as abundant as N-WASP but half as much as A36, the viral protein ultimately initiating actin tail formation. Overall, there appears to be a 4:2:1 ratio for the A36:Nck:N-WASP signalling network in MEFs. These values are consistent with the 2:1 ratio for Nck:N-WASP determined from modelling and live cell imaging of artificially clustered Nck SH3 domain on the plasma membrane (Ditlev et al.
222 2012). Our analysis goes beyond ratios as it now provides absolute numbers for Nck and N-WASP as well as A36, the activator of the signalling network.

Speed of virus depends on the level of Nck and not N-WASP

Previous studies have taken advantage of the known structure of viruses to generate fluorescence calibration standards by tagging defined numbers of viral capsid proteins with
228 (Dundr et al. 2002; Jose et al. 2015; Murray 2017). More recently, engineered nanocages with different numbers of GFP molecules have been used to provide quantitative insights into N-WASP and Arp2/3-driven endocytosis in yeast and human cells (Akamatsu et al. 2020; Sun et al. 2019). Using a similar imaging approach, we find that CEV inducing actin polymerization in MEFs recruit just over 400 molecules of N-WASP. This value is considerably higher than the maximum N-WASP numbers measured for endocytic patches in yeast (budding yeast 102 and
234 fission yeast 138) (Sun et al. 2019). Interestingly, however, in human cells, ~200 copies of the Arp2/3 complex are recruited during clathrin-mediated endocytic events (Akamatsu et al. 2020). Previous biochemical and structural analysis demonstrate that N-WASP dimers are more efficient at activating Arp2/3 and that the complex contains two N-WASP binding sites (Higgs & Pollard 2000; Padrick et al. 2011; Zimmet et al. 2020). This would suggest that an endocytic site in human cells will also recruit ~400 N-WASP molecules, which is similar to the
240 values we have observed associated with CEV. However, the area under a CEV is considerably larger than an invaginating endocytic pit which are typically 60-100 nm in diameter in human cells (Vigers et al. 1986; Yang et al. 2022). Based on our recent measurements of virion dimensions in cryo-electron tomographs of infected cells, the area under a CEV, which corresponds to the outer membrane of IEV, is 405,037 nm^2 (Hernandez-Gonzalez et al. 2022). This value is ~ 13x higher than the surface of an invaginating endosome (based on a radius of
246 50 nm). This suggests that the density of the signalling network beneath CEV is significantly less than that of an endocytic patch.

Loss of Grb2 or intersectin recruitment leads to even lower levels of N-WASP (245±26 and 276±66 respectively). However, the system does not collapse, and virus motility even increases. Moreover, while the levels of N-WASP are similar, in the absence of intersectin
252 (A36△NPF) the virus moves significantly faster than when Grb2 is absent (A36-Y132F). The striking difference between these two mutant viruses is the level of Nck recruited to the CEV, with the numbers being 61% lower for the A36△NPF mutant compared to the wild-type virus. Nck and N-WASP are both essential for Vaccinia induced actin polymerization, but how their

relative levels impact on the rate of actin-based motility is not established. Previous analysis reveals the density of artificially clustered VCA, the N-WASP domain responsible for activating
258 Arp2/3, does not affect downstream actin-based motility (Borinskaya et al. 2016). Interestingly, the same group also found that increasing the density of artificially clustered Nck SH3 domains on the plasma membrane increases the motility of actin structures (Ditlev et al. 2012). In their model system, Nck is permanently attached to the plasma membrane and not free to exchange as under CEV. This may underlie the difference in the trends of our observations. However, together with these previous studies, our data indicate that Nck
264 numbers and density are a critical determinant of actin-based motility in cells.

Why do Nck numbers impact Vaccinia motility? N-WASP/WASP activates Arp2/3 mediated actin polymerization more efficiently when acting as a dimer (Higgs & Pollard 2000; Padrick et al. 2008; Padrick et al. 2011; Zimmet et al. 2020). Previous simulations based on results from in vitro experiments suggests that when a protein that would dimerize N-WASP is high,
270 the probability of two N-WASP molecules engaging the same dimerizer is low (Padrick et al. 2008). Namely, each dimerizer would have a single N-WASP, which would be less efficient at stimulating the actin nucleating activity of the Arp2/3 complex. When the dimerizer concentration is optimal, it is more likely that two N-WASP molecules will interact with the same dimerizer making actin nucleation is more efficient. Our previous in vitro pulldown experiments demonstrated that two of the three SH3 domains in Nck were capable of binding
276 to N-WASP suggesting that this adaptor can function as a dimerizer. Thus, it is possible that the increase in the velocity of the A36△NPF virus is due to the concentration of Nck being closer to the optimal level required to fully dimerize N-WASP, making actin nucleation more efficient. It remains to be established why the lack of intersectin recruitment by A36 affects the levels of Nck so profoundly. The loss of the A36 NPF motifs results in reduced clustering of A36 (Humphries et al. 2012), which is expected to reduce the local density of Nck under
282 CEV. However, it should not reduce the total number of Nck molecules. We therefore favour a hypothesis that the absence of intersectin results in the loss of an unknown Nck stabilizing protein in addition to Cdc42 and AP2/clathrin.

288 **Implications of A36 density under CEV**

A36 that is present in the plasma membrane beneath CEV particles contains a single helical transmembrane domain, which is estimated to be approximately 1.2 nm wide. Assuming that no membrane is lost, and proteins do not diffuse significantly when IEVs fuse with the plasma membrane, our data indicate that A36 is present at a density of 0.2-0.5 molecules per 100 nm^2 based on the outer surface of 405,037 nm^2 for IEV. Interestingly, it has been determined
294 that 5800 molecules of the actin nucleating protein ActA of Listeria are present on the surface of the bacterium (Footer et al. 2008). The bacterial surface area is substantially larger than the membrane beneath CEV, however, the density of ActA molecules (0.09-0.3 molecules/100nm^2) is in a similar range to that of A36 (Footer et al. 2008).

Unexpectedly, we found that the number of A36 molecules associated with CEV varies
300 depending on the cell type. It can also be influenced by the length of infection. This is not the case with B5, which appears to remain relatively constant. The reason for the variation in A36 numbers is not clear, but it might be related to its level of expression in the infected cell (Fig 4E). Moreover, the variation in A36 suggests that viral protein composition in membranes around IEV, the outer one of which becomes incorporated into the plasma membrane below the CEV maybe not be fixed for all viral proteins. Consistent with this,
306 previous analysis reveals that ~ one third of extra-cellular enveloped virions (EEV) lack A56, an integral IEV membrane protein (Krauss et al. 2002; Smith et al. 2002).

Previous biochemical pulldowns and immunoprecipitations approaches have demonstrated that there are multiple interactions between IEV membrane proteins including A33:B5 (Chan & Ward 2012a,b; Perdiguero & Blasco 2006), A34:B5 (Earley et al. 2008; Monticelli et al. 2019;
312 Röttger et al. 1999), A34:A36 (Röttger et al. 1999), A33:A36 (Röttger et al. 1999; Ward et al. 2003; Wolffe et al. 2001), A36:F12 (Johnston & Ward 2009) and F12:E2 (Dodding et al. 2009; Van Vliet et al. 2009). These multiple associations suggest that the viral proteins likely form an immobile lattice within the membrane. Our measurement of the number of A36, B5 and F13 molecules in CEV is an important step in fully determining the precise organization of proteins in the viral membrane. B5 and F13 are present in the membrane surrounding CEV
318 as well as together with A36 in the plasma membrane beneath CEV. Assuming B5 and F13 are equally partitioned between the two membranes, then the levels of B5 and F13 are 1.3

and 3.8 fold higher than A36 beneath the CEV. It is striking that the levels of A36 and B5 are similar given there in no evidence that these proteins associate with each other (Van Vliet et al. 2009). Given their interactions, it will be interesting to measure the levels of A34 and A33. If the levels of A33 and A34, which are also integral membrane proteins are comparable to A36 and/or B5 it would suggest that the viral protein density in membranes around IEV is surprisingly low. In addition, the absence of an immobile viral protein lattice may explain why clathrin is able to cluster A36 after IEV fuse with the plasma membrane (Humphries et al. 2012).

In summary, our quantitative approach in determining precise numbers of molecules at CEV has unexpectedly revealed that A36 levels in the viral membrane are variable. It has also demonstrated that the velocity of virus movement depends on Nck rather than N-WASP which activates Arp2/3 complex dependent actin polymerization.

FIGURE LEGENDS

Figure 1: CEV and the signalling network that induces actin polymerisation

354 A schematic showing localisation of the vaccinia virus proteins A36, B5 and F13 in cell associated enveloped virions (CEV) on the plasma membrane. A36 and B5 are integral membrane proteins, while F13 associates with the membrane via lipidation. Inset shows the signalling network recruited by the cytoplasmic tail of A36 inducing actin polymerisation. Tyr112 and Tyr132 in A36, when phosphorylated by Src and Abl family kinases, recruit the adaptor proteins Nck and Grb2. Nck and Grb2 interact with N-WASP, which results in the
360 activation of the Arp2/3 complex and stimulation of actin polymerisation. NPF motifs in the C-terminus of A36 recruit the RhoGEF intersectin which recruits AP2/clathrin and also activates Cdc42 so it can bind N-WASP. While Nck is essential for actin tail formation, Grb2 and Cdc42 are not. Molecules labelled in green have been quantitatively analysed in this study.

366 **Figure 2: Determining the number of A36 molecules on CEV inducing actin polymerisation**

A. Representative single-plane spinning disc confocal image of a live HeLa cell stably expressing LifeAct-iRFP and infected with a recombinant virus expressing A36-TagGFP2 and RFP-A3 at their endogenous locus. The image is acquired at 9 hours post-infection. Scale bars = 10 µm. **B.** Representative single-plane confocal images comparing fluorescence intensity of A36-TagGFP2 at virus particles with TagGFP2-labeled 60mer nanocages in live HeLa cells.
372 Scale bar = 3 µm. **C.** Representative inverted average-intensity Z-projections of TagGFP2-tagged nanocages transiently expressed in live HeLa cells treated with 500 nM AP21967. Images were acquired at 100ms exposure. 60mers were imaged at 4x exposure to generate "240mer" intensities and 120mers were imaged at 3x exposure to generate "360mer" intensities. Scale bar = 2 µm. The graph shows quantification of background-subtracted raw integrated fluorescence intensities of nanocages. Linear line of regression is fitted to data
378 from 24-, 60-, 120- and 180mers. A total of 47-110 membrane-tethered nanocages were measured per condition over three independent experiments. A detailed version of the experimental data used to generate the calibration curve (green shaded area) is shown in Fig S2A. **D.** Representative inverted average-intensity Z-projections of A36-TagGFP2 at virus particles generating actin tails in live HeLa cells. Images were acquired at indicated exposure times. Coloured arrowheads indicate individual virus particles. Single-plane images in the

384 lower panel show positions of each particle 5 seconds after the Z-stack acquisition. Actin is labelled with LifeAct-iRFP, and all virus particles are labelled with RFP-A3. Scale bar = 2 µm. The graph shows quantification of background-subtracted raw integrated A36-TagGFP2 intensities at actin-polymerising virus particles, overlaid on the calibration curve generated in panel C. A total of 50-57 virions were measured per condition over three independent experiments. All error bars represent S.D and the distribution of data from each experiment
390 is shown using a "SuperPlot". The table shows the calculated number of A36 molecules on CEV inducing actin tails in HeLa cells (s.e.m. = standard error of mean).

Figure 3: Determining the number of B5 and F13 molecules on CEV inducing actin tails

A. Representative single-plane confocal images of live HeLa cells infected with a recombinant virus expressing B5-TagGFP2 or TagGFP2-F13 at their endogenous loci. Actin is labelled with
396 LifeAct-iRFP, and all virus particles are labelled with RFP-A3. Images are acquired at 9 hours post-infection. Scale bar = 10 µm. **B.** Representative inverted average-intensity Z-projections of A36-TagGFP2, B5-TagGFP2 and TagGFP2-F13 at virus particles generating actin tails in live HeLa cells. Coloured arrowheads indicate individual virus particles. Single-plane images in the right panel show positions of each particle 5 seconds after the Z-stack acquisition. Actin is labelled with LifeAct-iRFP, and all virus particles are labelled with RFP-A3. Scale bar = 2 µm.
402 **C.** The top graph shows quantification of background-subtracted raw integrated TagGFP2 intensities at actin-polymerising virions. All error bars represent S.D and the distribution of data from each experiment is shown using a "SuperPlot". A total of 39-54 particles were measured per recombinant virus over three independent experiments. The lower graph shows average measurements for each molecule superimposed on the calibration curve generated in Fig 2C. The table shows the calculated number of A36, B5 and F13 molecules at
408 actin-polymerising virus particles in HeLa cells (s.e.m. = standard error of mean).

Figure 4: Comparing numbers of A36 and B5 at CEV across host cell types

A and **B.** Representative inverted average-intensity Z-projections of A36-TagGFP2 (**A**) and B5-TagGFP2 (**B**) at virus particles generating actin tails in the indicated cell lines. Coloured arrowheads indicate individual virus particles. Single-plane images in the lower panels show
414 positions of these particles 5 seconds after the Z-stack acquisition. Actin is labelled with LifeAct-iRFP (stably expressed in HeLa and transiently expressed in other cell types). All virus

particles are labelled with RFP-A3. Scale bar = 2 µm. The graphs show quantification of background-subtracted raw integrated TagGFP2 intensities at actin-polymerising virus particles. All error bars represent S.D and the distribution of data from each experiment is shown using a "SuperPlot". A total of 29-62 (A36) or 26-41 (B5) particles were measured per
420 condition over three independent experiments. Tukey's multiple comparison's test was used to determine statistical significance; ns, $p > 0.05$; * $p \leq 0.05$. **C.** Table showing the calculated number of A36 and B5 molecules at virions inducing actin tails in the different host cell lines. **D.** Graph showing quantification of background-subtracted raw integrated A36-TagGFP2 intensities at actin-polymerising virus particles at 8- and 16-hours post-infection (hpi) in HeLa and N-WASP MEF host cells. All error bars represent S.D and the distribution of data from
426 each experiment is shown using a "SuperPlot". A total of 48-62 particles were measured per condition over three independent experiments. Tukey's multiple comparison's test was used to determine statistical significance; ns, $p > 0.05$; ** $p \leq 0.01$. **E.** Immunoblot analyses of total cell lysates from WR-infected HeLa and N-WASP MEF cells at 8- and 16-hours post-infection (hpi) respectively. N1 and vinculin represent viral and host protein loading controls.

432 **Figure 5: Determining the number of Nck and N-WASP molecules on CEV**

A. Representative immunofluorescence images showing the recruitment of N-WASP to actin tails in Vaccinia-infected MEF cells expressing TagGFP2-N-WASP in a N-WASP-null background or parental wildtype cells at 16 hours post-infection. N-WASP was detected with an antibody and actin is stained with phalloidin. Scale bar = 1 µm. **B.** Representative immunofluorescence images showing the recruitment of Nck to actin tails in Vaccinia-infected MEF cells expressing
438 TagGFP2-Nck in a Nck-null background or parental wildtype cells at 16 hours post-infection. Nck was detected with an antibody and actin is stained with phalloidin. Scale bar = 1 µm. **C.** Representative inverted average-intensity Z-projections of TagGFP2-Nck and TagGFP2-N-WASP in live Vaccinia WR-infected MEF cells stably expressing the corresponding tagged protein in Nck1/Nck2 -/- and N-WASP-/- backgrounds respectively. Images are taken at 16 hours post-infection. Scale bar = 10 µm. **D.** The graph shows quantification of background-
444 subtracted raw integrated TagGFP2 intensities at actin-polymerising virus particles. All error bars represent S.D and the distribution of data from each experiment is shown using a "SuperPlot". A total of 71-85 virions were measured per condition over three independent

experiments. The table shows the calculated number of Nck and N-WASP molecules at actin-polymerising virus particles in MEF cells.

450 **Figure 6: Nck and N-WASP are reduced On CEV in absence of Grb2 and intersectin**

A. Representative inverted average-intensity Z-projections of TagGFP2-Nck and TagGFP2-N-WASP at virus particles generating actin tails in live MEF cells infected with Vaccinia Western Reserve virus (WR) or the indicated A36 mutants. Pink arrow heads indicate particles generating actin tails as discerned by a transiently expressed LifeAct-iRFP and RFP A3 which labels viral cores. The LifeAct-iRFP and RFP-A3 channels are not shown for clarity. Scale bar =
456 10 µm. **B.** Graphs showing quantification of background-subtracted raw integrated intensities of TagGFP2-Nck and TagGFP2-N-WASP at actin-polymerising A36 mutant virus particles. All error bars represent S.D and the distribution of data from each experiment is shown using a "SuperPlot". A total of 34-49 (Nck) or 41-85 (N-WASP) particles were measured per condition over three independent experiments. Dunnett's multiple comparison's test was used to determine statistical significance; ns, $p > 0.05$; * $p \leq 0.05$. The table shows the calculated
462 number of Nck and N-WASP molecules at actin-polymerising virus particles in the indicated A36 mutants. **C.** Temporal colour-coded representation of time-lapse movies tracking the motility of the indicated RFP-A3-labelled virus over 50 seconds in HeLa cells at 8 hours post infection. Images were recorded every second and the position of virus particles at frame 1 (open triangles) and frame 50 (white triangles) are indicated. Scale bar = 3 µm. The graph shows quantification of virus speed. All error bars represent S.D and the distribution of data
468 from each experiment is shown using a "SuperPlot". A total of 31-51 tracks were analysed per condition over three independent experiments. Dunnett's multiple comparison's test was used to determine statistical significance; ns, $p > 0.05$; ** $p \leq 0.01$.

474

SUPPORTING INFORMATION

480 **Supplement 1: Validation TagGFP2-labelled recombinant viruses**

A. Immunoblot analyses of total cell lysates from HeLa cells infected with Vaccinia WR or the indicated TagGFP2 fusion viruses at 9 hours post-infection. **B.** Representative images of plaques produced by the indicated viruses in confluent BS-C-1 cells at 72 hours post-infection. Scale bar = 2 mm**.** The graph shows quantification of plaque diameter of the recombinant viruses compared with WR. The graph on the right shows that the RFP-A3 tag that labels the
486 virus core does not confer a change in plaque diameter. All error bars represent S.D and the distribution of data from each experiment is shown using a "SuperPlot". A total of 36 plaques per virus were measured over three independent experiments. Dunnett's multiple comparison's test (left graph) or Welch's t test (right graph) was used to determine statistical significance; ns, $p > 0.05$; * $p \leq 0.05$; ** $p \leq 0.01$.

492 **Supplement 2: Validation of fluorescent nanocages**

A. The graph shows quantification of background-subtracted raw integrated fluorescence intensities of nanocages transiently expressed in live HeLa cells treated with 500 nM AP21967. Linear line of regression is fitted to the data. A total of 47-110 membrane-tethered nanocages were measured per condition over three independent experiments. **B.** Quantification of background-subtracted raw integrated intensity of 60mer TagGFP2-
498 nanocages transiently expressed in HeLa cells or N-WASP+/+ parental MEFs treated with 500 nM AP21967. A total of 66-84 membrane-tethered spots were measured over three independent experiments. All error bars represent S.D and the distribution of data from each experiment is shown using a "SuperPlot". Welch's t test (panel B) was used to determine statistical significance; ns, $p > 0.05$.

504 **Supplement 3: Validation of stable cell lines expressing TagGFP2-Nck and TagGFP2-N-WASP**

A. Immunoblot analyses of total cell lysates from Nck1/Nck2 null MEFs with and without stable expression of TagGFP2-Nck together with parental wild-type cells. **B.** Immunoblot analyses of total cell lysates from N-WASP null MEFs with and without stable expression of TagGFP2-N-WASP together with parental wild-type cells. Immunoblot analyses was performed with the indicated antibodies. ** indicates the band corresponding to the
510 TagGFP2-labelled protein.

MATERIALS AND METHODS:

Expression constructs and targeting vectors

The expression vector pE/L-LifeAct-iRFP670 and the plasmid for the 180-mer nanocage was previously made in the Way lab (Galloni et al. 2021; Xu et al. 2022). Plasmids for 12-, 24-, 60- and 120-mer TagGFP2 nanocage expression were obtained from the Drubin lab (Akamatsu et
516 al. 2020). All other expression constructs generated for this study were made using Gibson Assembly (New England Biolabs) according to manufacturer's instructions. All primers used in cloning are listed in Table 1. The lentiviral expression constructs pLVX-TagGFP2-Nck and pLVX-TagGFP2-N-WASP were generated by cloning a TagGFP2 fragment into ApaI/NotI sites of pLVX-GFP-Nck (Basant & Way 2022) and pLVX-GFP-N-WASP (Donnelly et al. 2013) respectively. The A36-TagGFP2 construct was made by assembling the fusion fragment and
522 cloning into NotI/HindIII sites of a A36 targeting vector (Basant & Way 2022). The B5-TagGFP2 construct was made by cloning a TagGFP2 fragment into NotI/XbaI sites of a B5-YFP targeting vector (Dodding et al. 2009). To generate the TagGFP2-F13 targeting vector, the F13 gene and 423bp of upstream and downstream sequences were amplified from the WR strain of Vaccinia virus genomic DNA. This was assembled with a TagGFP2 fragment and cloned into NotI/HindIII sites of pBS SKII. SnapGene software (from Insightful Science; available
528 at snapgene.com) was used to plan and visualise cloning strategies, and to analyse sequencing results.

Table 1. Primers

No.	***Sequence***	***Construct(s)***
AB123	TCGACGGTACCGCGGGCCCATGGGAGGCGAAGAGCTGTTTGCTG	pLVX-TagGFP2-Nck pLVX-TagGFP2-N-WASP
AB124	TGCCATTCCTCCGCGGCCGCCTGTCCCGGAACCTGCCCT	pLVX-TagGFP2-Nck
AB125	GCCGCCGCCGCGGCCGCCTGTCCCGGAACCTGCCCT	pLVX-TagGFP2-N-WASP
AB084	GTCGTATCATTGGTGGGGTCGGGGTCGGATCCACCGGTCGCCACCG GAGGCGAAGAGCTGTTT	pBS SKII A36-TagGFP2
AB085	GTCGTATCATTGGTGGGGTCGGGGTCGGATCCACCGGTCGCCACCG GAGGCGAAGAGCTGTTT	pBS SKII A36-TagGFP2
AB086	GCAGGTTCCGGGACATAATTAGTTTCCTTTTTATAAAATTGAAG	pBS SKII A36-TagGFP2
AB052	GGTCGACGGTATCGATAAGCTTTATCTATAGAGATAACAC	pBS SKII A36-TagGFP2

MHG055	ATTGGAGCTCCACCGCGGTGGCGGCCGCCGCCATCGTCGGTGTGTTGTC	pBS SKII TagGFP2-F13
AB135	GCAAACAGCTCTTCGCCTCCCATTTAGTTAACATAAAAACTTA	pBS SKII TagGFP2-F13
AB136	TAAGTTTTTATGTTAACTAAATGGGAGGCGAAGAGCTGTTTGC	pBS SKII TagGFP2-F13
AB137	GTACCGATGCAAATGGCCACATGCGGCCGCCTGTCCCGGAACCTGCCCT	pBS SKII TagGFP2-F13
AB131	AGGGCAGGTTCCGGGACATAAATATAAATCCGTTAAAATAA	pBS SKII B5-TagGFP2
AB132	TCCCCGCGGGTGGGCGCTCTAGAACTAGTGGGATCCTATACCATT	pBS SKII B5-TagGFP2
AB133	ATTGCTACCGGGCGGCGCGGCCGCCGGAGGCGAAGAGCTGTTTGC	pBS SKII B5-TagGFP2
AB134	TTATTTTAACGGATTTATATTTATGTCCCGGAACCTGCCCT	pBS SKII B5-TagGFP2

Cell lines

534 HeLa cells were maintained in minimal essential medium (MEM) and MEFs and A549 cells were maintained in Dulbecco's Modified Eagle Medium (DMEM). All cells were supplemented with 10% FBS, 100 U/ml penicillin, and 100 µg/ml streptomycin at 37°C and 5% CO_2. The HeLa cell line stably expressing LifeAct-iRFP670 (Snetkov et al. 2016) was previously generated in the Way lab. Nck -/- MEFs (Bladt et al. 2003) and N-WASP-/-MEFs (Snapper et al. 2001) were provided by the late Tony Pawson (Samuel Lunenfeld Research Institute, Toronto, Canada)
540 and Scott Snapper (Harvard Medical School, Boston, MA) respectively. A549 cells were obtained from ATCC. For this study, lentiviral expression vectors were used to stably express TagGFP2-Nck in Nck-/- MEFs and TagGFP2-N-WASP in N-WASP-/- MEFs. All cell lines were generated using the lentivirus Trono group second generation packaging system (Addgene) and selected using puromycin resistance (2 µg/ml) as previously described (Abella et al. 2016). Expression of the relevant fusion proteins was confirmed by live imaging and immunoblot
546 analysis (Fig S3). The following primary antibodies were used: anti-Nck (BD transduction; 1:1000), anti-vinculin (Sigma #V4505; 1:2000), anti-N-WASP (Cell Signalling #4848S; 1:1000), anti-TagGFP2 antibody (Evrogen #AB121; 1:3000). HRP-conjugated secondary antibodies were purchased from The Jackson Laboratory.

Viral plaque assays

552 Plaque assays were performed in confluent BS-C-1 cell monolayers. Cells were infected with the relevant Vaccinia virus at a multiplicity of infection (MOI) = 0.1 in serum-free MEM for

one hour. The inoculum was replaced with a semi-solid overlay consisting of a 1:1 mix of MEM and 2% carboxymethyl cellulose. Cells were fixed with 3% formaldehyde at 72 hours post-infection and subsequently visualized with crystal violet cell stain as previously described (Humphries et al. 2012). To determine plaque size, the diameter of well-separated plaques
558 was measured using the Fiji line tool (Schindelin et al. 2012).

Construction of recombinant Vaccinia viruses

In this study, recombinant Vaccinia viruses expressing A36-TagGFP2, B5-TagGFP2 or TagGFP2-F13 at their endogenous loci were generated in a parental WR viral strain expressing RFP-A3. Recombinants were isolated by selecting viral plaques positive for TagGFP2 fluorescence as
564 described previously (Basant & Way 2022). To introduce relevant constructs into their genomic loci, HeLa cells infected with WR (RFP-A3) at MOI = 0.05 were transfected with the appropriate pBS SKII targeting vectors using Lipofectamine2000 (Invitrogen) as described by the manufacturer. When all cells displayed cytopathic effect at 48-72 hours post-infection, they were lysed, and serial dilutions of the lysates were used to infect confluent BS-C-1 cell monolayers in a plaque assay (see above). RFP and TagGFP2 positive plaques were picked,
570 and plaque lysates were used to infect fresh BS-C-1 cell monolayers over at least three rounds of plaque purification. Successful recombination at the correct locus, loss of the parent variant and virus purity were verified by PCR, sequencing and immunoblot. The following primary antibodies were used: anti-vinculin (Sigma #V4505; 1:2000), anti-TagGFP2 (Evrogen #AB121; 1:3000), anti-N1 ((Postigo & Way 2012); 1:3000), anti-A36 ((Röttger et al. 1999); 1:3000), anti-B5 ((Schmelz et al. 1994); 1:5000), anti-F13L-N ((Rietdorf et al. 2001); 1:5000).
576 HRP-conjugated secondary antibodies were purchased from The Jackson Laboratory. For all experiments, recombinant viruses were purified through a sucrose cushion before use and storage.

Vaccinia virus infection for imaging

For live and fixed cell imaging, cells plated on fibronectin-coated MatTek dishes (MatTek
582 corporation) or coverslips were infected with the relevant Vaccinia virus recombinant in serum-free MEM at MOI = 1. After one hour at 37°C, the serum-free MEM was removed and replaced with complete MEM. Cells were incubated at 37°C until further processing.

Transient transfection and drug treatment

All transfections prior to imaging were carried out using FUGENE (Promega) as described by
588 the manufacturer. To visualize filamentous actin in live cells, Vaccinia-infected A549 cells and MEFs were transiently transfected with pE/L-LifeAct-iRFP670 one hour after infection. Plasmids expressing nanocage constructs were transfected into HeLa cells or MEFs at least 16 hours prior to imaging along with a plasmid expressing cytosolic mCherry to easily identify transfected cells. To induce nanocage tethering to the plasma membrane, 500nM AP21967 (Takara) was added to the media at least 30 minutes prior to imaging.

594

Immunofluorescence

At 8 hours (HeLa) or 16 hours (MEFs) post-infection, cells were fixed with 4% paraformaldehyde in PBS for 10 min, blocked in cytoskeletal buffer (1 mM MES, 15 mM NaCl, 0.5 mM EGTA, 0.5 mM $MgCl_2$, and 0.5 mM glucose, pH 6.1) containing 2% (vol/vol) fetal calf serum and 1% (wt/vol) BSA for 30 min, and then permeabilized with 0.1% Triton-X/PBS for 5
600 min. To visualize cell-associated enveloped virions (CEV), cells were stained with, with a monoclonal antibody against B5 (19C2, rat, 1:1000; (Schmelz et al. 1994)) followed by an Alexa Fluor 647 anti-rat secondary antibody (Invitrogen; 1:1000 in blocking buffer) prior to permeabilization of the cells with detergent. Other primary antibodies used were anti-Nck (Millipore #06-288; 1:100) and anti-N-WASP (Cell Signalling #4848S; 1:100) followed by Alexa Fluor 568 conjugated secondary antibodies (Invitrogen; 1:1000 in blocking buffer). Actin tails
606 were labeled with Alexa Fluor 488 phalloidin (Invitrogen; 1:500). Coverslips were mounted on glass slides using Mowiol (Sigma). Coverslips were imaged on a Zeiss Axioplan2 microscope equipped with a 63x/1.4 NA Plan-Achromat objective and a Photometrics Cool Snap HQ cooled charge-coupled device camera. The microscope was controlled with MetaMorph 7.8.13.0 software.

612 **Live-cell imaging**

Live-cell imaging experiments were performed starting at 8 hours or 16 hours post-infection in complete MEM (10% FBS) in a temperature-controlled chamber at 37°C. For all molecule counting experiments, cells were imaged on a Zeiss Axio Observer spinning-disk microscope equipped with a Plan Achromat 100×/1.46 NA oil lens, an Evolve 512 camera, and a Yokagawa CSUX spinning disk. The microscope was controlled by the SlideBook software (3i Intelligent

618 Imaging Innovations). To generate a calibration curve using TagGFP2 nanocages, image stacks of ten Z-slices 0.1 µm apart were acquired using an exposure of 100ms (unless stated otherwise) for 10 seconds at 1 sec intervals. When quantifying TagGFP2 molecules at virus particles, a single Z stack was acquired followed by a single plane image of RFP (virus) and iRFP (LifeAct) channels to help identify virus particles generating actin tails. To determine virus speed, images were acquired using a 63x/1.4 Ph3 M27 oil lens in RFP (virus) and iRFP
624 (LifeAct) channels for 50 seconds at 1Hz.

Image analysis and quantitation

For molecule counting analysis, average intensity Z projections of GFP channel images were generated in Fiji. The ComDet v.0.5.5 plugin for ImageJ (https://github.com/UU-cellbiology/ComDet) was used to identify fluorescent spots and measure their background-
630 subtracted integrated intensity. Only tethered nanocages, that remained in frame over 10s of imaging, were used for analysis. Intensities obtained from 24-, 60-, 120-, 180-mers imaged at 100ms exposure were plotted as a function of predicted TagGFP2 number per nanocage. A line of linear fit through the origin was applied by linear least-squares fitting to generate the calibration curve used in this study. To calculate TagGFP2 numbers at Vaccinia CEV, fluorescent spots identified by the ComDet v.0.5.5 plugin were overlaid with RFP (virus)/iRFP
636 (actin) images to only select particles associated with actin tails.

To analyse virus motility, two-colour time-lapse movies of HeLa cells stably expressing LifeAct-iRFP670 infected with the relevant recombinant virus labelled with RFP-A3 were used. The velocity of virus particles in the RFP channel was measured using a Fiji plugin developed by David Barry (the Francis Crick Institute) as previously described (Basant & Way 2022).

642

Whole-cell lysate immunoblot

HeLa cells and MEFs infected with WR were lysed at 8- and 16-hours post-infection respectively in PBS containing 1% SDS, a cocktail of protease and phosphatase inhibitors (cOmplete (Roche), PHOSstop (Roche)) and Benzonase (Millipore). Proteins from these lysates were resolved on an SDS-PAGE and the levels of total B5 and A36 were determined by
648 immunoblot analysis using anti-A36 ((Röttger et al. 1999); 1:3000) and anti-B5 ((Schmelz et al. 1994); 1:5000). As loading controls, anti-vinculin (Sigma #V4505; 1:2000) and anti-N1

((Postigo & Way 2012); 1:3000) were used. HRP-conjugated secondary antibodies were purchased from The Jackson Laboratory.

Statistical analysis and figure preparation

All data are presented as means ± S.D. For all experiments, means of at least three independent experiments (i.e. biological replicates) were used to determine statistical significance by a Welch's t-test (comparing only two conditions), Tukey's multiple comparisons test (comparing multiple conditions with each other) or a Dunnett's multiple comparisons test (comparing multiple conditions with a control). All data are represented as SuperPlots to allow assessment of the data distribution in individual experiments (Lord et al. 2020). SuperPlots were generated using the SuperPlotsOfData webapp (Goedhart 2021) and GraphPad Prism 9. All data were analyzed using GraphPad Prism 9 or the SuperPlotsOfData webapp. Schematics were created with BioRender.com. Final figures were assembled using Keynote software.

ACKNOWLEDGEMENTS

We thank members of the Way Laboratory for useful discussions and suggestions. We thank David Drubin and Matthew Akamatsu (UC Berkeley) for sharing nanocage plasmids and helping optimize their imaging. We also thank David Barry (Francis Crick Institute) and Stephen J Royle (University of Warwick) for image analysis advice, and Miguel Hernández González (Way lab) for help in generating the TagGFP2-F13 expression construct. Special thanks to Jeremy Carlton and Snezhka Oliferenko (Francis Crick Institute) for helpful comments on the manuscript. Michael Way was supported by the Francis Crick Institute, which receives its core funding from Cancer Research UK (CC2096), the UK Medical Research Council (CC2096), and the Wellcome Trust (CC2096) For the purpose of Open Access, the authors have applied a CC BY public copyright license to any Author Accepted Manuscript version arising from this submission.

REFERENCES

Abella JVG, Galloni C, Pernier J, Barry DJ, Kjær S, et al. 2016. Isoform diversity in the Arp2/3 complex determines actin filament dynamics. *Nat. Cell Biol.* 18(1):76–86

Akamatsu M, Vasan R, Serwas D, Ferrin MA, Rangamani P, Drubin DG. 2020. Principles of self-organization and load adaptation by the actin cytoskeleton during clathrin-mediated endocytosis. *eLife*. 9:e49840

Basant A, Way M. 2022. The relative binding position of Nck and Grb2 adaptors impacts actin-based motility of Vaccinia virus. *eLife*. 11:e74655

Bladt F, Aippersbach E, Gelkop S, Strasser GA, Nash P, et al. 2003. The murine Nck SH2/SH3 adaptors are important for the development of mesoderm-derived embryonic structures and for regulating the cellular actin network. *Mol. Cell. Biol.* 23(13):4586–97

Blasco R, Moss B. 1991. Extracellular vaccinia virus formation and cell-to-cell virus transmission are prevented by deletion of the gene encoding the 37,000-Dalton outer envelope protein. *J. Virol.* 65(11):5910–20

Borinskaya S, Velle KB, Campellone KG, Talman A, Alvarez D, et al. 2016. Integration of linear and dendritic actin nucleation in Nck-induced actin comets. *Mol. Biol. Cell*. 27(2):247–59

Chan WM, Ward BM. 2012a. The A33-dependent incorporation of B5 into extracellular enveloped vaccinia virions is mediated through an interaction between their lumenal domains. *J. Virol.* 86(15):8210–20

Chan WM, Ward BM. 2012b. Increased interaction between vaccinia virus proteins A33 and B5 is detrimental to infectious extracellular enveloped virion production. *J. Virol.* 86(15):8232–44

Cudmore S, Cossart P, Griffiths G, Way M. 1995. Actin-based motility of vaccinia virus. *Nature*. 378(6557):636–38

708 Cudmore S, Reckmann I, Griffiths G, Way M. 1996. Vaccinia virus: a model system for actin-membrane interactions. *J. Cell Sci.* 109 (Pt 7):1739–47

Ditlev JA, Michalski PJ, Huber G, Rivera GM, Mohler WA, et al. 2012. Stoichiometry of Nck-dependent actin polymerization in living cells. *J. Cell Biol.* 197(5):643–58

Doceul V, Hollinshead M, van der Linden L, Smith GL. 2010. Repulsion of superinfecting virions: a mechanism for rapid virus spread. *Science*. 327(5967):873–76

714 Dodding MP, Mitter R, Humphries AC, Way M. 2011. A kinesin-1 binding motif in vaccinia virus that is widespread throughout the human genome. *EMBO J.* 30(22):4523–38

Dodding MP, Newsome TP, Collinson LM, Edwards C, Way M. 2009. An E2–F12 complex is required for intracellular enveloped virus morphogenesis during vaccinia infection. *Cell. Microbiol.* 11(5):808–24

Domi A, Weisberg AS, Moss B. 2008. Vaccinia virus E2L null mutants exhibit a major

720 reduction in extracellular virion formation and virus spread. *J. Virol.* 82(9):4215–26

Donnelly SK, Weisswange I, Zettl M, Way M. 2013. WIP provides an essential link between Nck and N-WASP during Arp2/3-dependent actin polymerization. *Curr. Biol.* 23(11):999–1006

Dundr M, McNally JG, Cohen J, Misteli T. 2002. Quantitation of GFP-fusion proteins in single living cells. *J. Struct. Biol.* 140(1):92–99

726 Earley AK, Chan WM, Ward BM. 2008. The vaccinia virus B5 protein requires A34 for efficient intracellular trafficking from the endoplasmic reticulum to the site of wrapping and incorporation into progeny virions. *J. Virol.* 82(5):2161–69

Engelstad M, Smith GL. 1993. The Vaccinia Virus 42-kDa Envelope Protein is Required for the Envelopment and Egress of Extracellular Virus and for Virus Virulence. *Virology*. 194(2):627–37

732 Footer MJ, Lyo JK, Theriot JA. 2008. Close Packing of Listeria monocytogenes ActA, a Natively Unfolded Protein, Enhances F-actin Assembly without Dimerization. *J. Biol. Chem.* 283(35):23852–62

Frischknecht F, Moreau V, Röttger S, Gonfloni S, Reckmann I, et al. 1999. Actin-based motility of vaccinia virus mimics receptor tyrosine kinase signalling. *Nature*. 401(6756):926–29

738 Galloni C, Carra D, Abella JVG, Kjær S, Singaravelu P, et al. 2021. MICAL2 enhances branched actin network disassembly by oxidizing Arp3B-containing Arp2/3 complexes. *J. Cell Biol.* 220(8):1–28

Geada MM, Galindo I, Lorenzo MM, Perdiguero B, Blasco R. 2001. Movements of vaccinia virus intracellular enveloped virions with GFP tagged to the F13L envelope protein. *J. Gen. Virol.* 82(11):2747–60

744 Goedhart J. 2021. SuperPlotsOfData—a web app for the transparent display and quantitative comparison of continuous data from different conditions. *Mol. Biol. Cell*. 32:470–74

Hernandez-Gonzalez M, Calcraft T, Nans A, Rosenthal PB, Way M. 2022. Cryo-ET of infected cells reveals that a succession of two lattices drives vaccinia virus assembly. *bioRxiv.* 10.1101/2022.08.11.503617

750 Higgs HN, Pollard TD. 2000. Activation by Cdc42 and Pip_2 of Wiskott-Aldrich Syndrome Protein (Wasp) Stimulates Actin Nucleation by Arp2/3 Complex. *J. Cell Biol.* 150(6):1311–20

Hollinshead M, Rodger G, Van Eijl H, Law M, Hollinshead R, et al. 2001. Vaccinia virus utilizes microtubules for movement to the cell surface. *J. Cell Biol.* 154(2):389–402

Humphries AC, Dodding MP, Barry DJ, Collinson LM, Durkin CH, Way M. 2012. Clathrin potentiates vaccinia-induced actin polymerization to facilitate viral spread. *Cell Host Microbe*. 12(3):346–59

Humphries AC, Donnelly SK, Way M. 2014. Cdc42 and the Rho GEF intersectin-1 collaborate with Nck to promote N-WASP-dependent actin polymerisation. *J. Cell Sci.* 127(Pt 3):673–85

Johnston SC, Ward BM. 2009. Vaccinia Virus Protein F12 Associates with Intracellular Enveloped Virions through an Interaction with A36. *J. Virol.* 83(4):1708–17

Jose J, Tang J, Taylor AB, Baker TS, Kuhn RJ. 2015. Fluorescent Protein-Tagged Sindbis Virus E2 Glycoprotein Allows Single Particle Analysis of Virus Budding from Live Cells. *Viruses*. 7(12):6182–99

Krauss O, Hollinshead R, Hollinshead M, Smith GL. 2002. An investigation of incorporation of cellular antigens into vaccinia virus particles. *J. Gen. Virol.* 83(Pt 10):2347–59

Leite F, Way M. 2015. The role of signalling and the cytoskeleton during Vaccinia Virus egress. *Virus Res.* 209:87–99

Lord SJ, Velle KB, Mullins RD, Fritz-Laylin LK. 2020. SuperPlots: Communicating reproducibility and variability in cell biology. *J. Cell Biol.* 219(6):94–10

Monticelli SR, Earley AK, Tate J, Ward BM. 2019. The Ectodomain of the Vaccinia Virus Glycoprotein A34 Is Required for Cell Binding by Extracellular Virions and Contains a Large Region Capable of Interaction with Glycoprotein B5. *J. Virol.* 93(4):a010199-21

Moreau V, Frischknecht F, Reckmann I, Vincentelli R, Rabut G, et al. 2000. A complex of N-WASP and WIP integrates signalling cascades that lead to actin polymerization. *Nat. Cell Biol.* 2:441–48

Murray JM. 2017. An icosahedral virus as a fluorescent calibration standard: methods for counting protein molecules in cells by fluorescence microscopy. . 267(2):193–213

780 Newsome TP, Scaplehorn N, Way M. 2004. Src Mediates a Switch from Microtubule- to Actin-Based Motility of Vaccinia Virus. *Science*. 306(5693):124–29

Newsome TP, Weisswange I, Frischknecht F, Way M. 2006. Abl collaborates with Src family kinases to stimulate actin-based motility of vaccinia virus. *Cell. Microbiol.* 8(2):233–41

Padrick SB, Cheng H-C, Ismail AM, Panchal SC, Doolittle LK, et al. 2008. Hierarchical

786 Regulation of WASP/WAVE Proteins. *Mol. Cell*. 32(3):426–38

Padrick SB, Doolittle LK, Brautigam CA, King DS, Rosen MK. 2011. Arp2/3 complex is bound and activated by two WASP proteins. *Proc. Natl. Acad. Sci.* 108(33):E472–79

Perdiguero B, Blasco R. 2006. Interaction between vaccinia virus extracellular virus envelope A33 and B5 glycoproteins. *J. Virol.* 80(17):8763–77

Pernigo S, Lamprecht A, Steiner RA, Dodding MP. 2013. Structural Basis for Kinesin-1:Cargo

792 Recognition. *Science*. 340(6130):356–59

Postigo A, Way M. 2012. The Vaccinia Virus-Encoded Bcl-2 Homologues Do Not Act as Direct Bax Inhibitors. *J. Virol.* 86(1):203–13

Reeves PM, Bommarius B, Lebeis S, McNulty S, Christensen J, et al. 2005. Disabling poxvirus pathogenesis by inhibition of Abl-family tyrosine kinases. *Nat. Med.* 11(7):731–39

Rietdorf J, Ploubidou A, Reckmann I, Holmström A, Frischknecht F, et al. 2001. Kinesin-dependent movement on microtubules precedes actin-based motility of vaccinia virus. *Nat. Cell Biol.* 3(11):992–1000

Röttger S, Frischknecht F, Reckmann I, Smith GL, Way M. 1999. Interactions between vaccinia virus IEV membrane proteins and their roles in IEV assembly and actin tail formation. *J. Virol.* 73(4):2863–75

Sanderson CM, Frischknecht F, Way M, Hollinshead M, Smith GL. 1998. Roles of vaccinia virus EEV-specific proteins in intracellular actin tail formation and low pH-induced cell-cell fusion. *J. Gen. Virol.* 79 (Pt 6):1415–25

Sanderson CM, Hollinshead M, Smith GL. 2000. The vaccinia virus A27L protein is needed for the microtubule-dependent transport of intracellular mature virus particles. *J. Gen. Virol.* 81(1):47–58

Scaplehorn N, Holmström A, Moreau V, Frischknecht F, Reckmann I, Way M. 2002. Grb2 and Nck Act Cooperatively to Promote Actin-Based Motility of Vaccinia Virus. *Curr. Biol.* 12:740–45

Schindelin J, Arganda-Carreras I, Frise E, Kaynig V, Longair M, et al. 2012. Fiji: an open-source platform for biological-image analysis. *Nat. Methods*. 9(7):676–82

Schmelz M, Sodeik B, Ericsson M, Wolffe EJ, Shida H, et al. 1994. Assembly of Vaccinia Virus: the Second Wrapping Cisterna Is Derived From the Trans Golgi Network. *J. Virol.* 68(1):130–47

Smith GL, Vanderplasschen A, Law M. 2002. The formation and function of extracellular enveloped vaccinia virus. *J. Gen. Virol.* 83(12):2915–31

Snapper SB, Takeshima F, Anton I, Liu C-H, Thomas SM, et al. 2001. N-WASP deficiency reveals distinct pathways for cell surface projections and microbial actin-based motility. *Nat. Cell Biol.* 3:897–904

822 Snetkov X, Weisswange I, Pfanzelter J, Humphries AC, Way M. 2016. NPF motifs in the vaccinia virus protein A36 recruit intersectin-1 to promote Cdc42:N-WASP-mediated viral release from infected cells. *Nat. Microbiol.* 1(10):16141

Sun Y, Schöneberg J, Chen X, Jiang T, Kaplan C, et al. 2019. Direct comparison of clathrin-mediated endocytosis in budding and fission yeast reveals conserved and evolvable features. *eLife*. 8:e50749

828 Tooze J, Hollinshead M, Reis B, Radsak K, Kern H. 1993. Progeny vaccinia and human cytomegalovirus particles utilize early endosomal cisternae for their envelopes. *Eur. J. Cell Biol.* 60(1):163–78

van Eijl H, Hollinshead M, Smith GL. 2000. The Vaccinia Virus A36R Protein Is a Type Ib Membrane Protein Present on Intracellular but Not Extracellular Enveloped Virus Particles. *Virology*. 271(1):26–36

834 Van Vliet K, Mohamed MR, Zhang L, Villa NY, Werden SJ, et al. 2009. Poxvirus proteomics and virus-host protein interactions. *Microbiol. Mol. Biol. Rev.* 73(4):730–49

Vigers GP, Crowther RA, Pearse BM. 1986. Location of the 100 kd-50 kd accessory proteins in clathrin coats. *EMBO J.* 5(9):2079–85

Ward BM. 2005. Visualization and characterization of the intracellular movement of vaccinia virus intracellular mature virions. *J. Virol.* 79(8):4755–63

840 Ward BM, Moss B. 2001a. Vaccinia Virus Intracellular Movement Is Associated with Microtubules and Independent of Actin Tails. *J. Virol.* 75(23):11651–63

Ward BM, Moss B. 2001b. Visualization of Intracellular Movement of Vaccinia Virus Virions Containing a Green Fluorescent Protein-B5R Membrane Protein Chimera. *J. Virol.* 75(10):4802–13

Ward BM, Moss B. 2004. Vaccinia Virus A36R Membrane Protein Provides a Direct Link between Intracellular Enveloped Virions and the Microtubule Motor Kinesin. *J. Virol.* 78(5):2486–93

Ward BM, Weisberg AS, Moss B. 2003. Mapping and functional analysis of interaction sites within the cytoplasmic domains of the vaccinia virus A33R and A36R envelope proteins. *J. Virol.* 77(7):4113–26

Weisswange I, Newsome TP, Schleich S, Way M. 2009. The rate of N-WASP exchange limits the extent of ARP2/3-complex-dependent actin-based motility. *Nature*. 458(7234):87–91

Wolffe EJ, Isaacs SN, Moss B. 1993. Deletion of the vaccinia virus B5R gene encoding a 42-kilodalton membrane glycoprotein inhibits extracellular virus envelope formation and dissemination. *J. Virol.* 67(8):4732–41

Wolffe EJ, Weisberg AS, Moss B. 1998. Role for the Vaccinia Virus A36R Outer Envelope Protein in the Formation of Virus-Tipped Actin-Containing Microvilli and Cell-to-Cell Virus Spread. *Virology*. 244(1):20–26

Wolffe EJ, Weisberg AS, Moss B. 2001. The vaccinia virus A33R protein provides a chaperone function for viral membrane localization and tyrosine phosphorylation of the A36R protein. *J. Virol.* 75(1):303–10

Xu A, Basant A, Schleich S, Newsome TP, Way M. 2022. Kinesin-1 transports morphologically distinct intracellular virions during vaccinia infection. *J. Cell Sci.* 136(5):jcs260175

Yang C, Colosi P, Hugelier S, Zabezhinsky D, Lakadamyali M, Svitkina T. 2022. Actin polymerization promotes invagination of flat clathrin-coated lattices in mammalian cells by pushing at lattice edges. *Nat. Commun.* 13:6127

Zettl M, Way M. 2002. The WH1 and EVH1 Domains of WASP and Ena/VASP Family Members Bind Distinct Sequence Motifs. *Curr. Biol.* 12(18):1617–22

Zimmet A, Van Eeuwen T, Boczkowska M, Rebowski G, Murakami K, Dominguez R. 2020. Cryo-EM structure of NPF-bound human Arp2/3 complex and activation mechanism. *Sci. Adv.* 6(23):eaaz7651

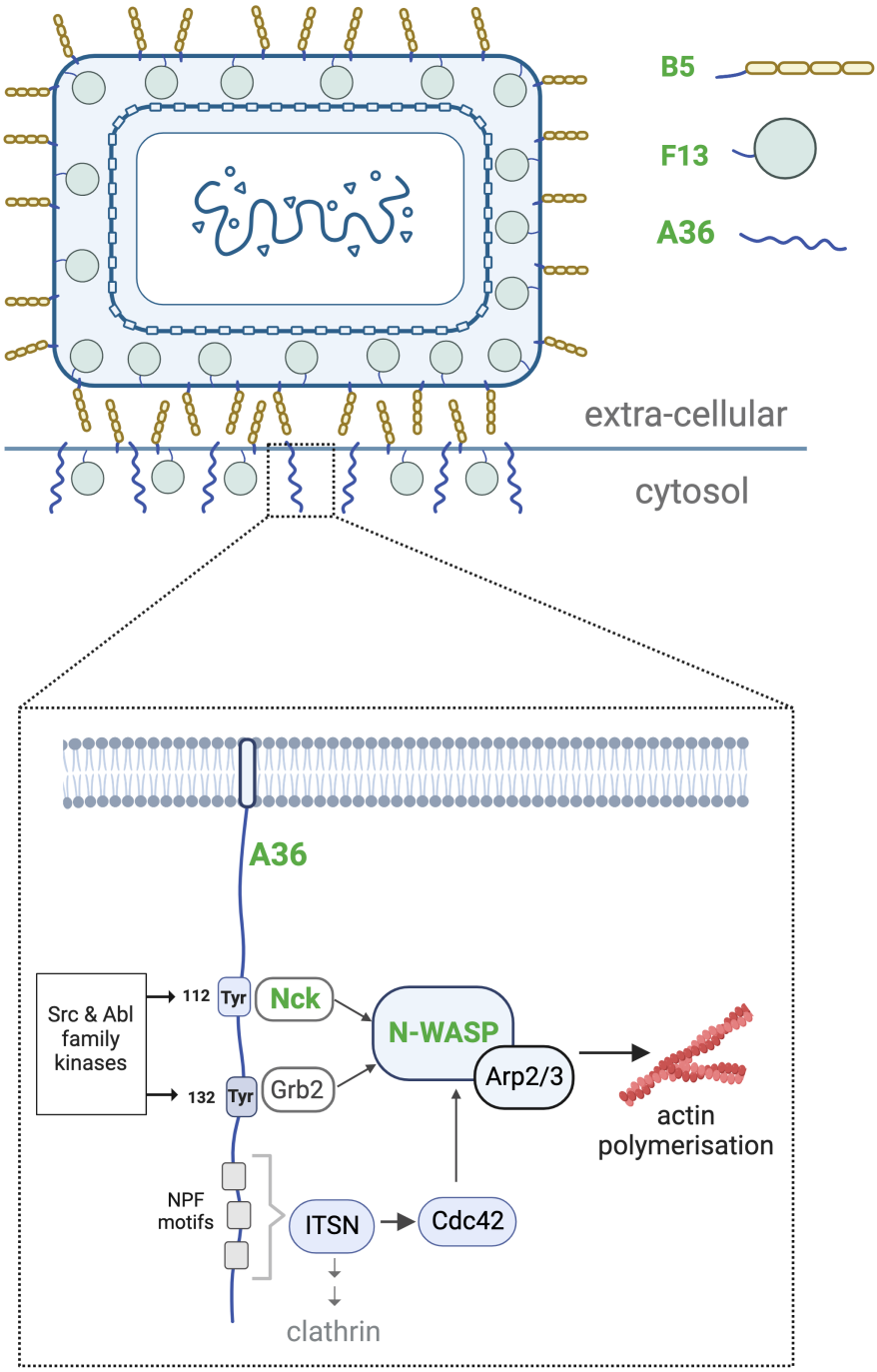
B5
F13
A36
extra-cellular
cytosol
A36
Src & Abl family kinases
112
Tyr
Nck
132
Tyr
Grb2
N-WASP
Arp2/3
actin polymerisation
NPF motifs
ITSN
Cdc42
clathrin

Figure 1

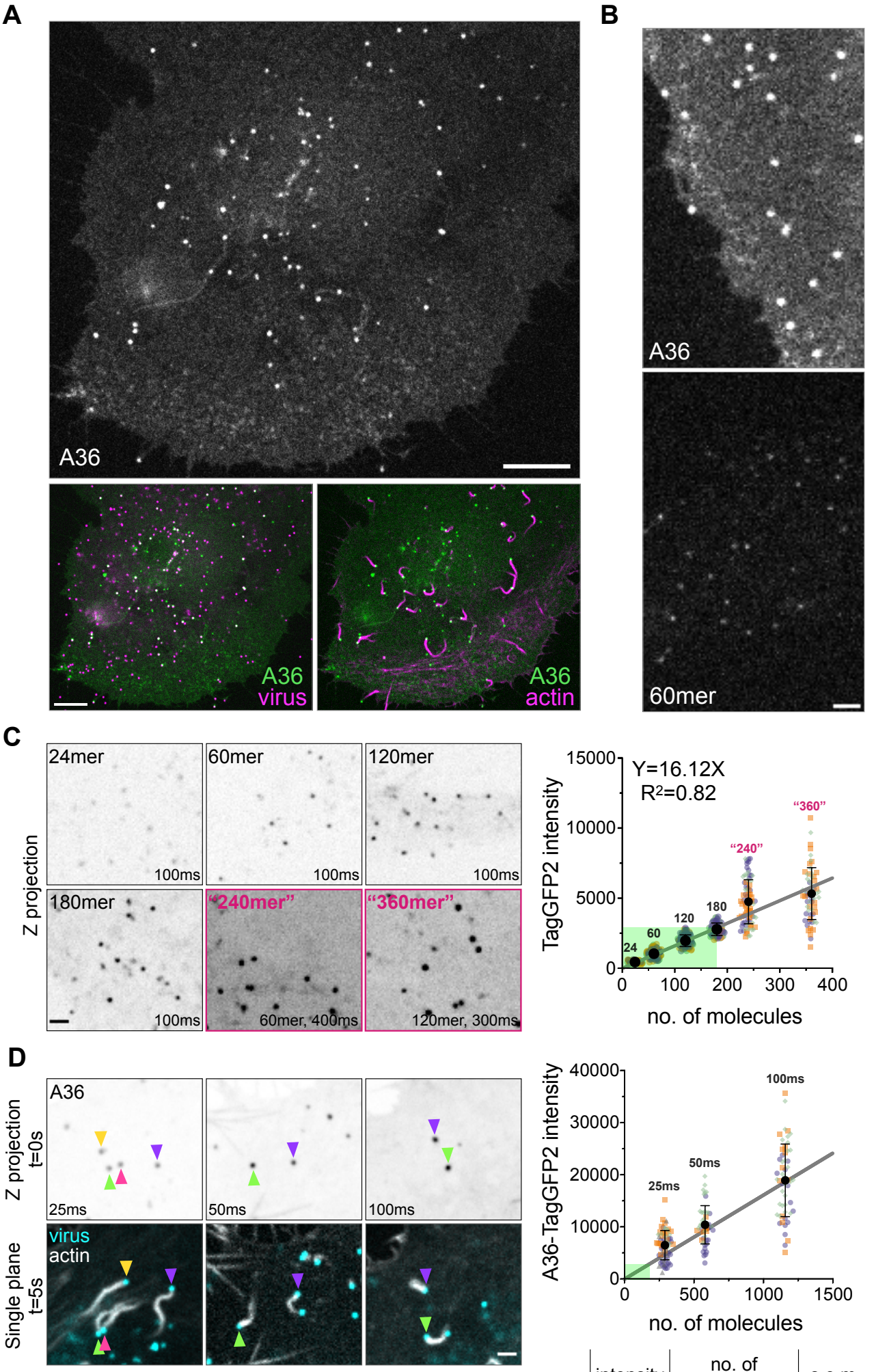

	intensity	no. of molecules	s.e.m.
A36	18632	1156	±120

Figure 2:

A

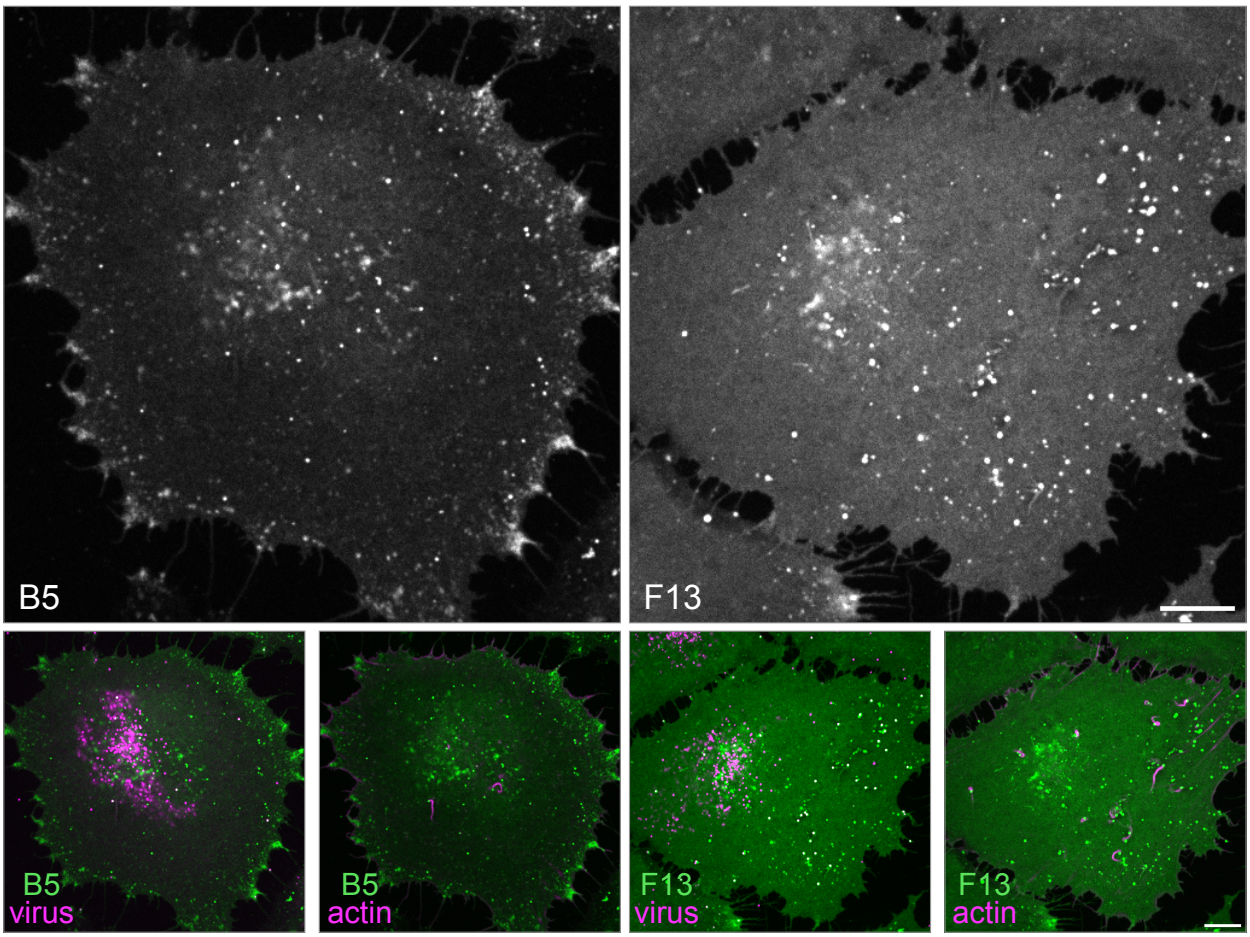

B

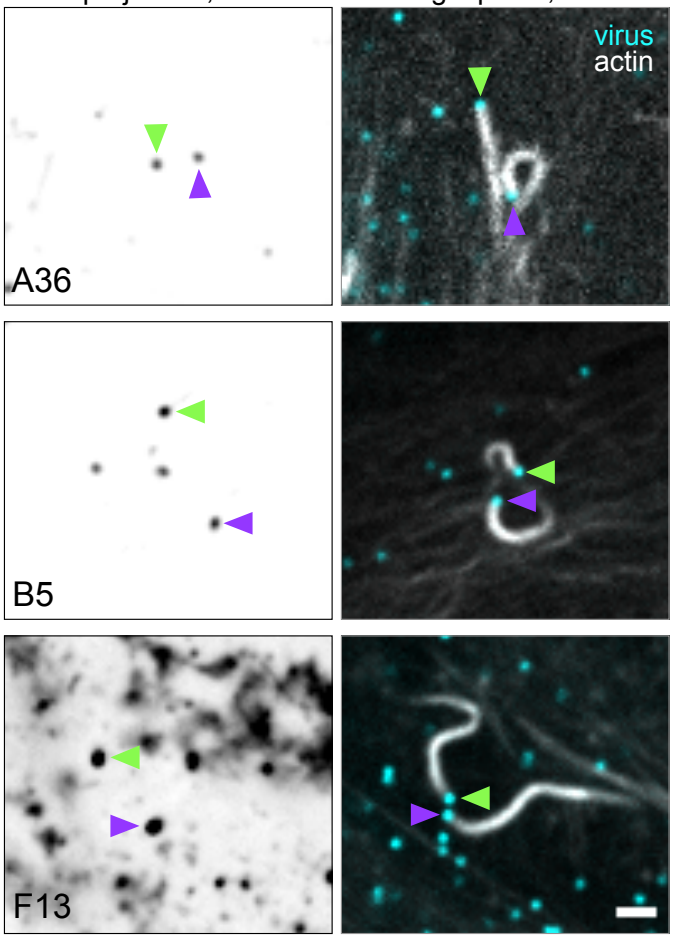

C

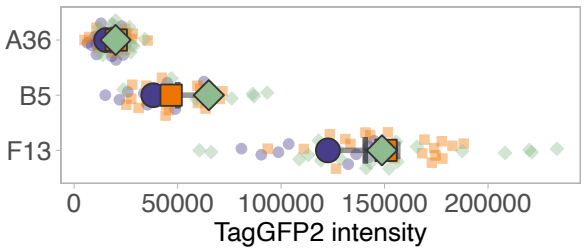

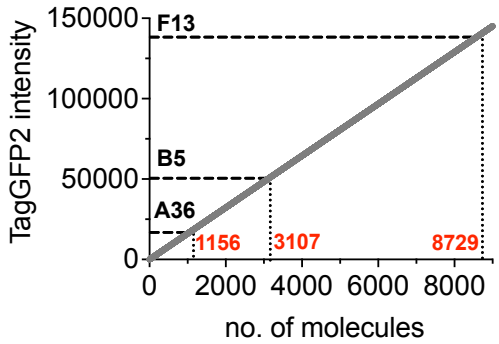

	intensity	no. of molecules	s.e.m.
A36	18632	1156	±120
B5	50079	3107	±602
F13	140707	8729	±688

Figure 3:

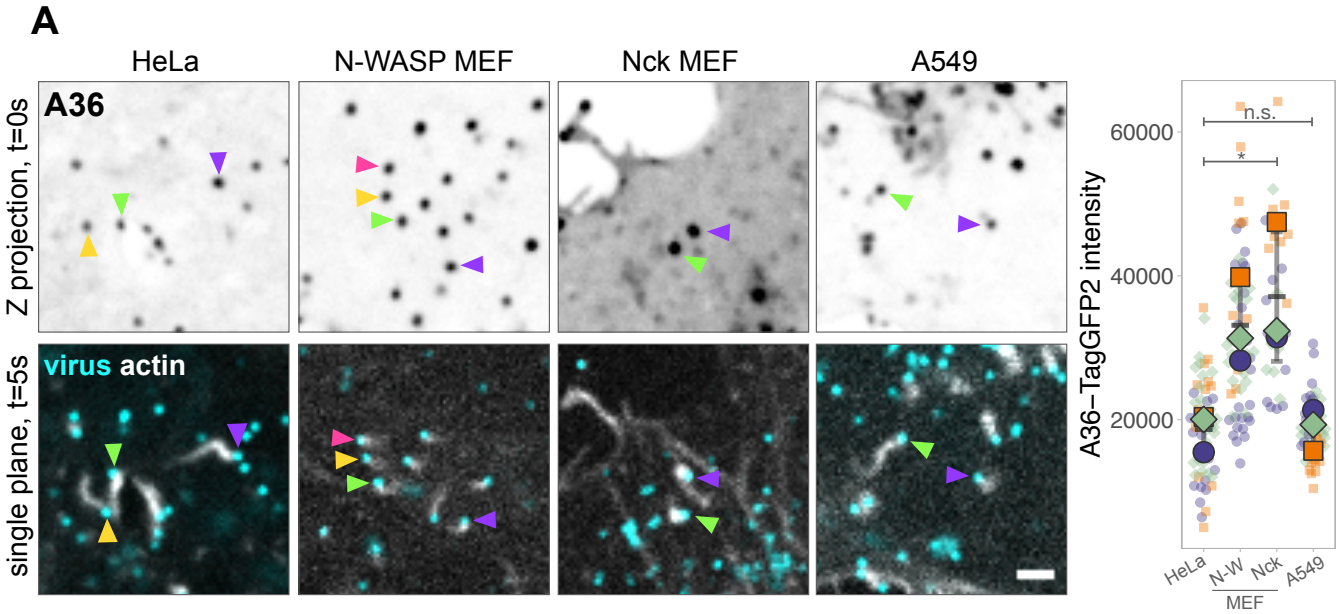

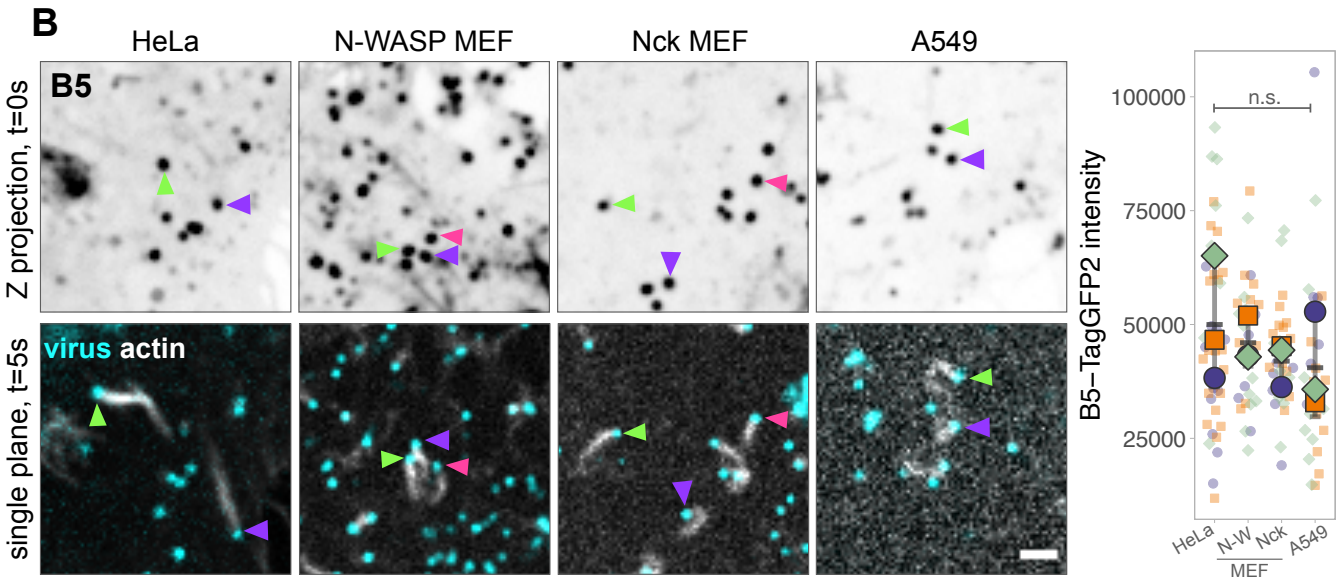

C

	cell type	intensity	no. of molecules	s.e.m.
A36	HeLa	18632	1156	±120
A36	N-WASP MEF	33128	2055	±263
A36	Nck MEF	37111	2302	±395
A36	A549	18782	1165	±126
B5	HeLa	50079	3107	±602
B5	N-WASP MEF	45999	2854	±227
B5	Nck MEF	41957	2603	±217
B5	A549	40504	2513	±472

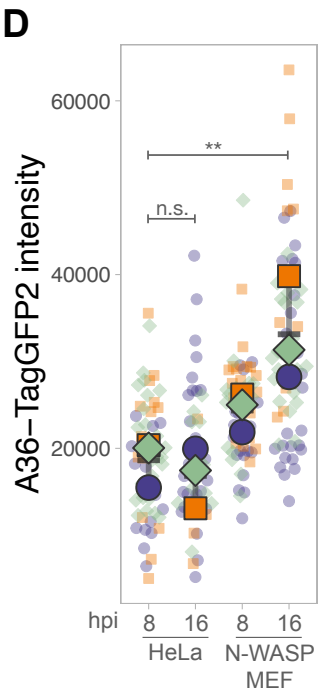

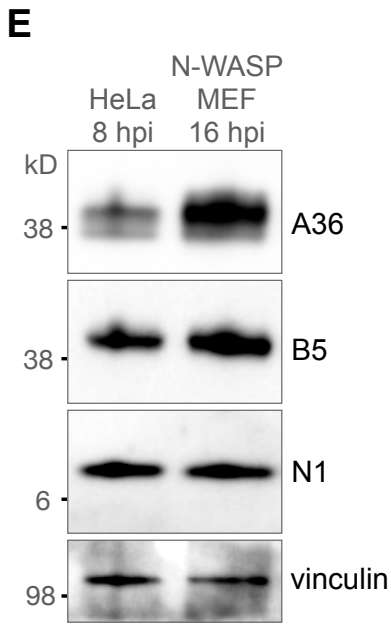

Fig 4:

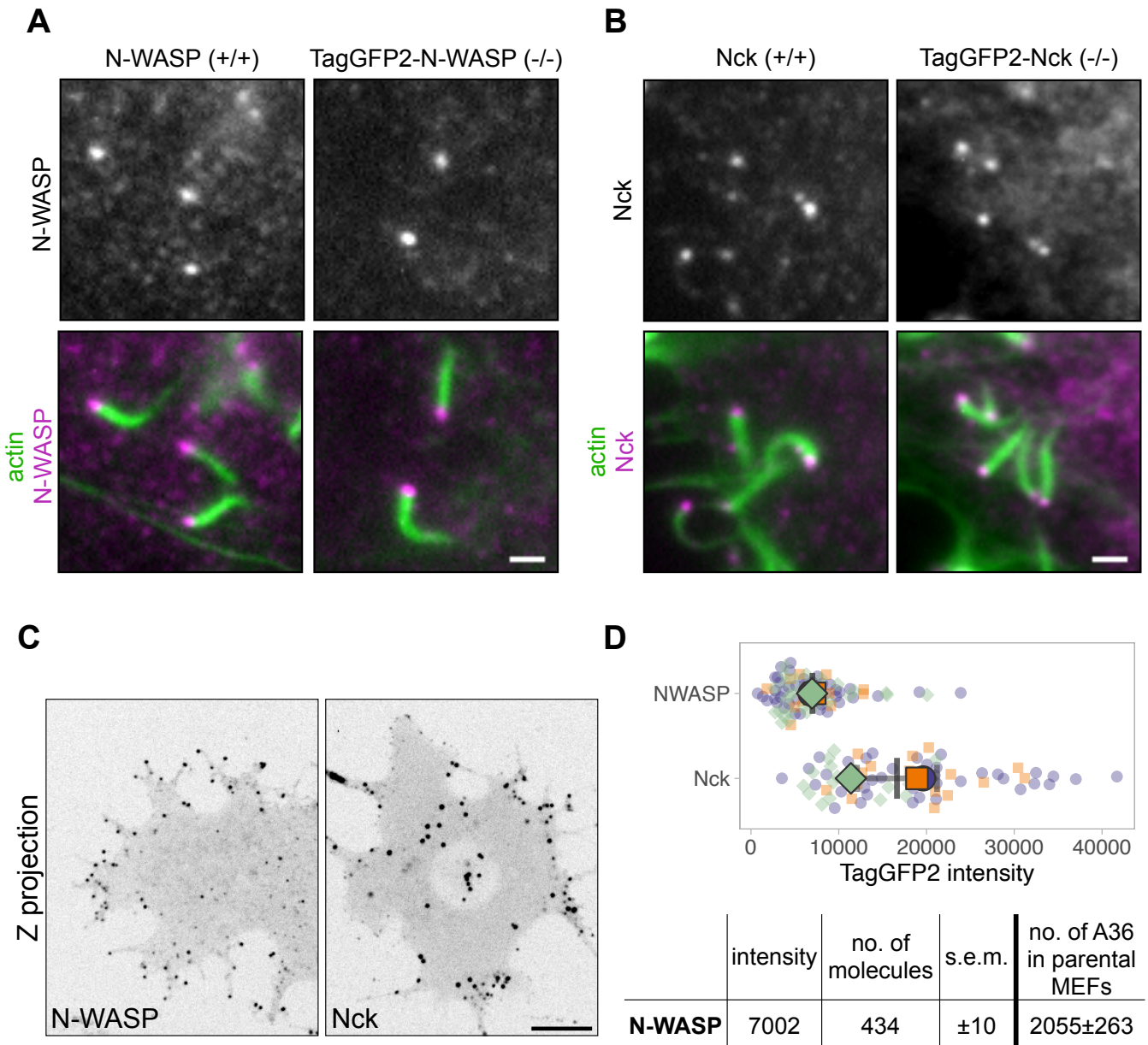

	intensity	no. of molecules	s.e.m.	no. of A36 in parental MEFs
N-WASP	7002	434	±10	2055±263
Nck	16637	1032	±200	2302±395

Figure 5:

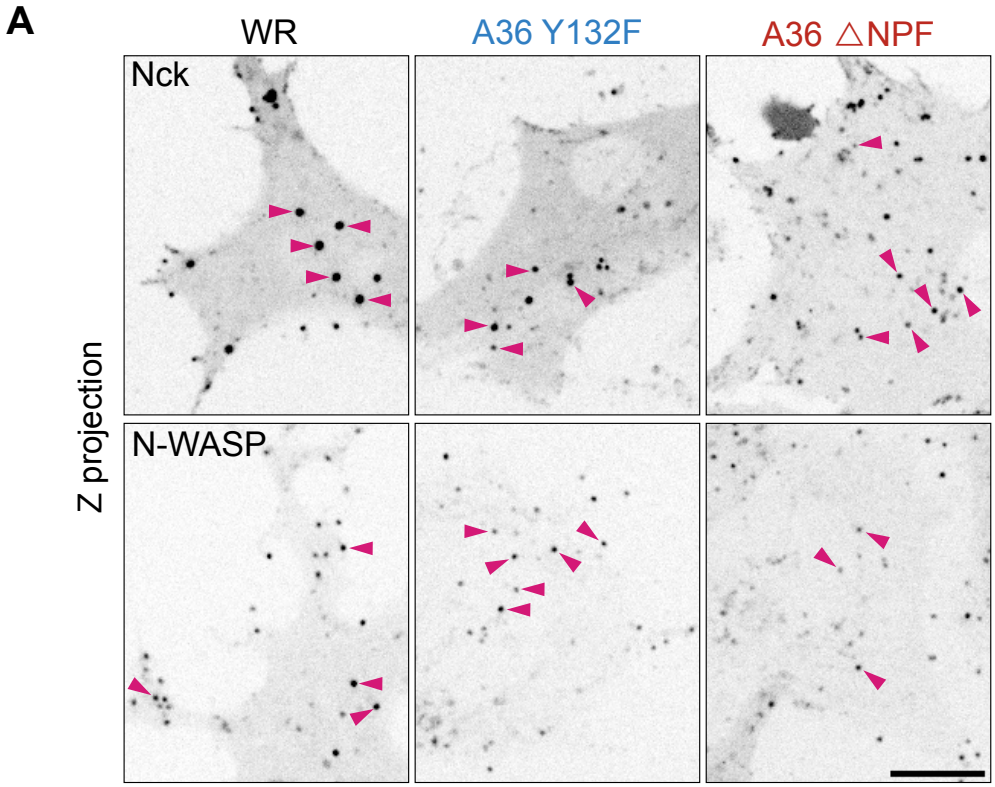

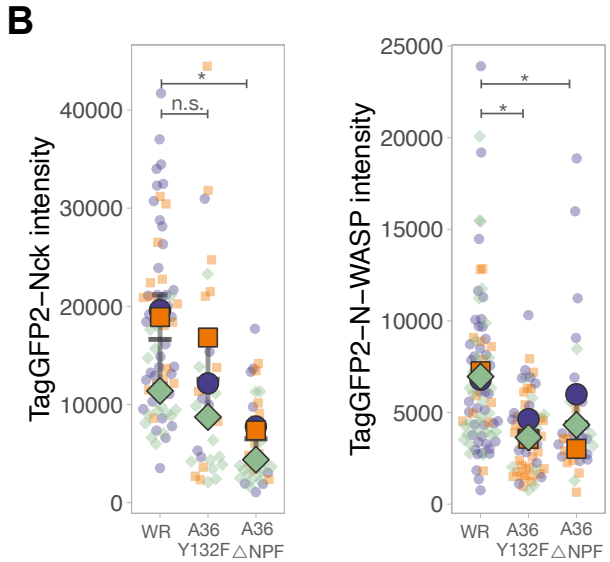

virus		intensity	no. of molecules	s.e.m.
WR	Nck	16637	1032	±200
A36 Y132F	Nck	12573	780	±178
A36 △NPF	Nck	6504	403	±55
WR	N-WASP	7002	434	±10
A36 Y132F	N-WASP	3948	245	±26
A36 △NPF	N-WASP	4447	276	±66

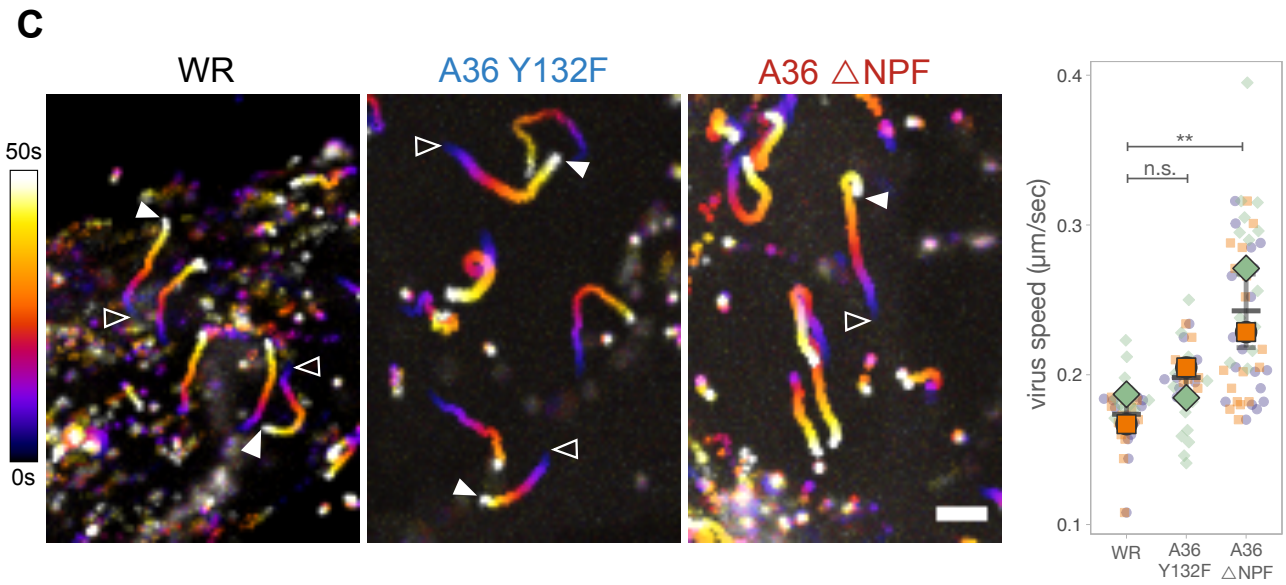

Fig 6:

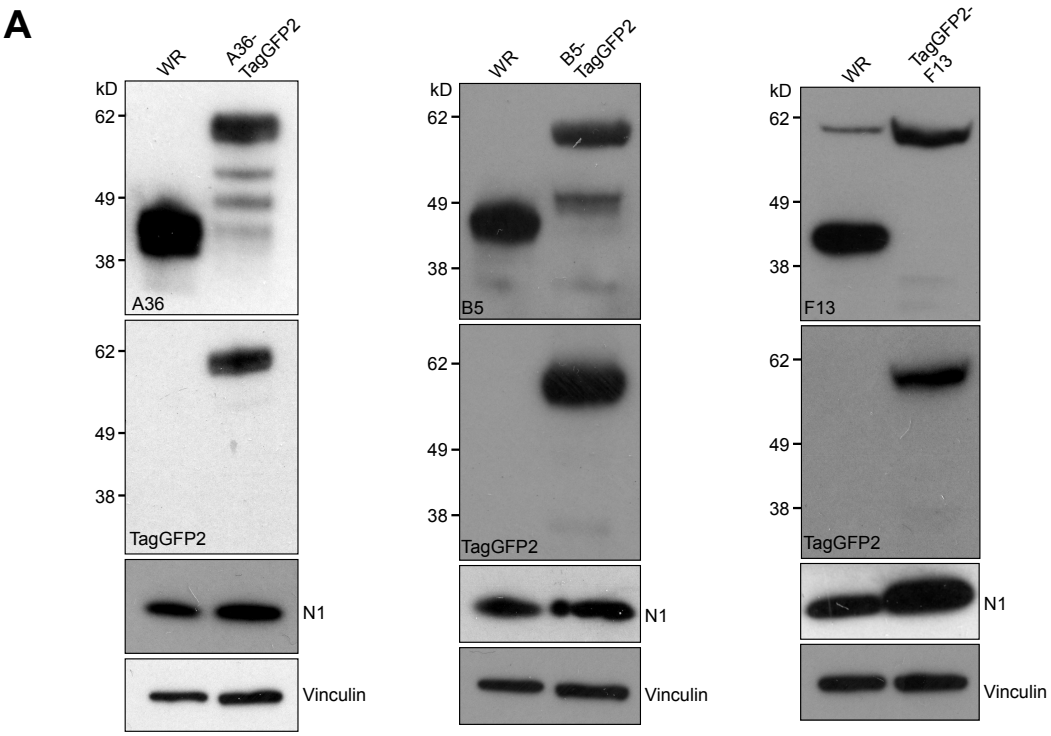
A
WR
A36-TagGFP2
B5-TagGFP2
TagGFP2-F13
kD
62
49
38
A36
B5
F13
TagGFP2
N1
Vinculin

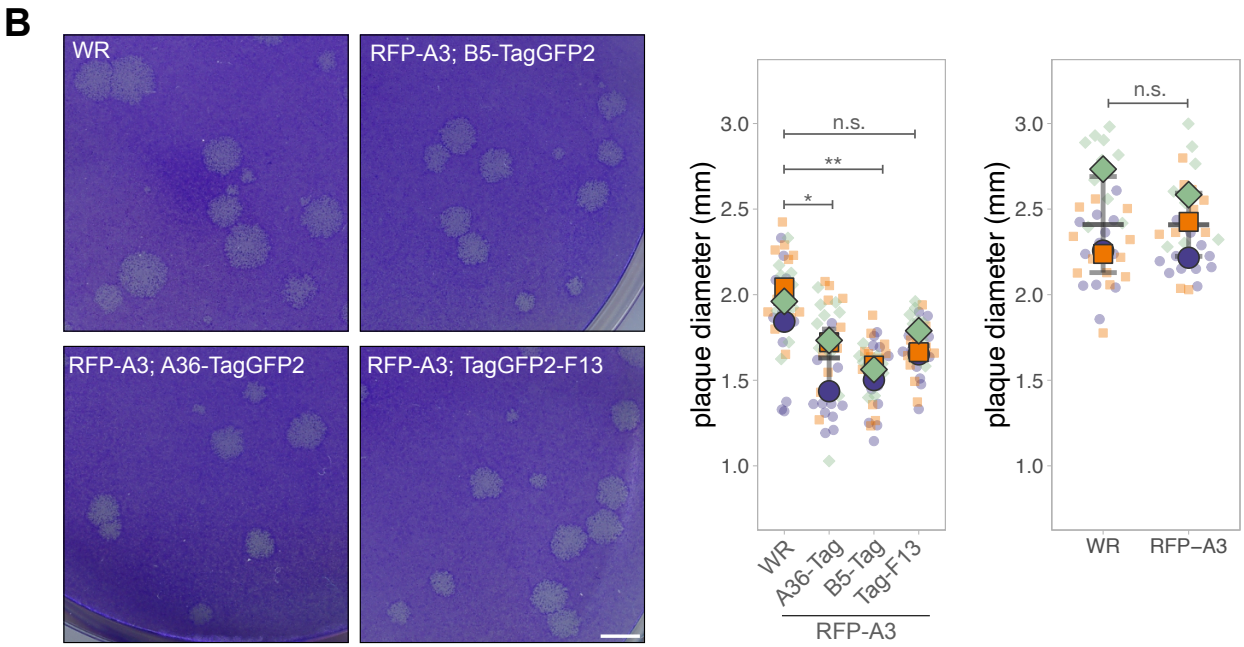
B
WR
RFP-A3; B5-TagGFP2
RFP-A3; A36-TagGFP2
RFP-A3; TagGFP2-F13
plaque diameter (mm)
3.0
2.5
2.0
1.5
1.0
n.s.
**
*
WR
A36-Tag
B5-Tag
Tag-F13
RFP-A3
RFP–A3

Suppl1:

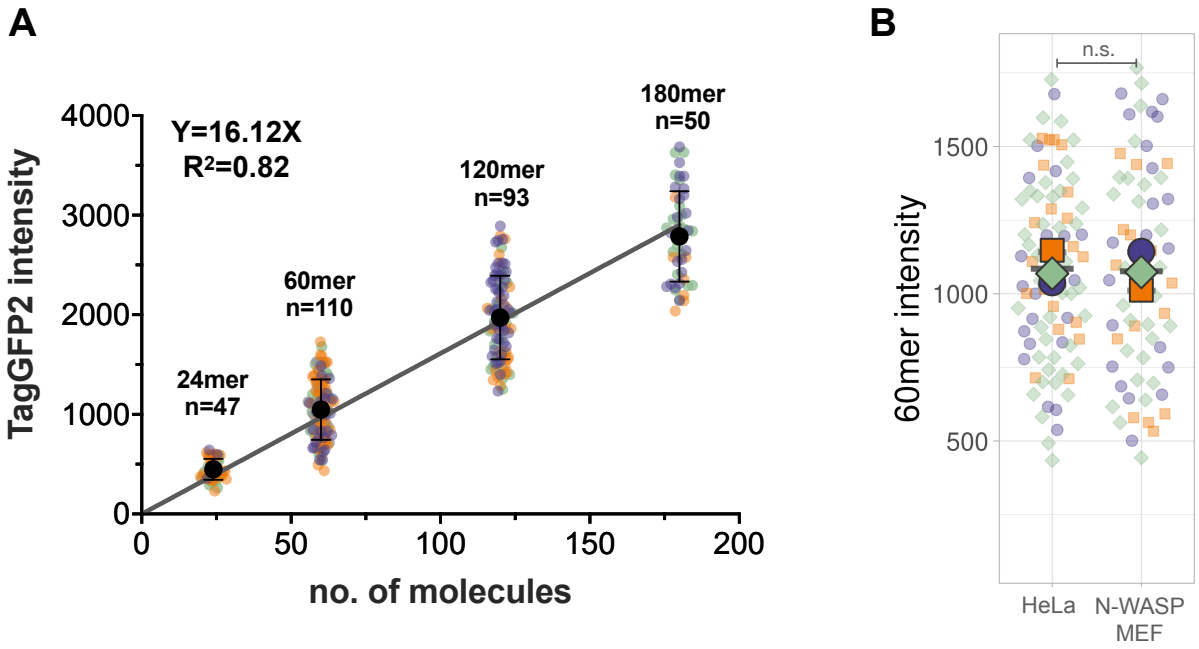
A
Y=16.12X
R²=0.82
TagGFP2 intensity
no. of molecules
24mer
n=47
60mer
n=110
120mer
n=93
180mer
n=50
0
1000
2000
3000
4000
0
50
100
150
200
B
n.s.
60mer intensity
1500
1000
500
HeLa
N-WASP
MEF

Suppl 2:

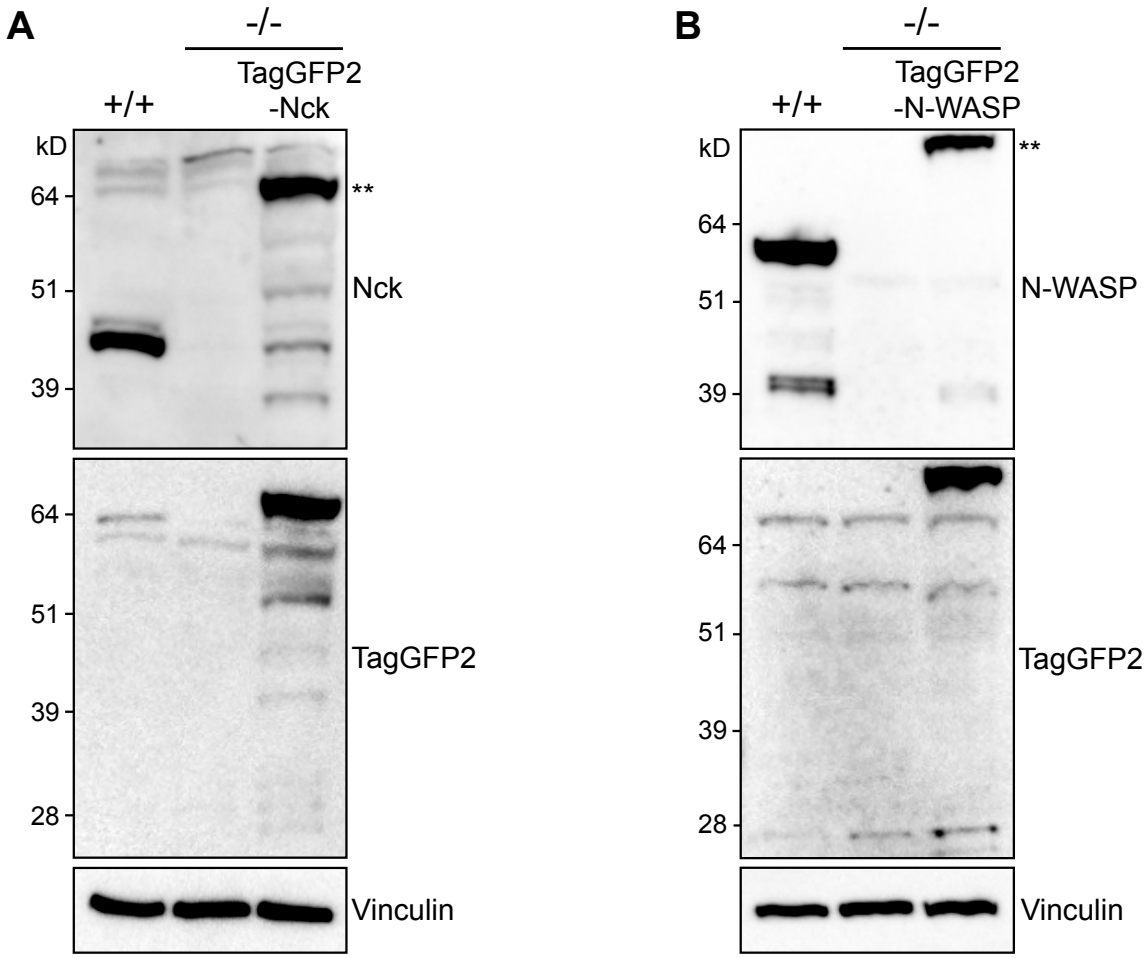
A
-/-
+/+
TagGFP2
-Nck
kD
64
51
39
**
Nck
64
51
39
28
TagGFP2
Vinculin
B
-/-
+/+
TagGFP2
-N-WASP
kD
64
51
39
**
N-WASP
64
51
39
28
TagGFP2
Vinculin

Suppl 3: